A&A 381, 32–50 (2002)
DOI: 10.1051/0004-6361:20011488

Astronomy & Astrophysics

Using Cepheids to determine the galactic abundance gradient

I. The solar neighbourhood ⋆,⋆⋆

S. M. Andrievsky[1,2], V. V. Kovtyukh[2,3], R. E. Luck[4,5], J. R. D. Lépine[1], D. Bersier[6], W. J. Maciel[1], B. Barbuy[1], V. G. Klochkova[7,8], V. E. Panchuk[7,8], and R. U. Karpischek[9]

[1] Instituto Astronômico e Geofísico, Universidade de São Paulo, Av. Miguel Stefano, 4200 São Paulo SP, Brazil
e-mail: sergei@andromeda.iagusp.usp.br
[2] Department of Astronomy, Odessa State University, Shevchenko Park, 65014, Odessa, Ukraine
e-mail: val@deneb.odessa.ua
[3] Odessa Astronomical Observatory and Isaac Newton Institute of Chile, Odessa Branch, Ukraine
[4] Department of Astronomy, Case Western Reserve University, 10900 Euclid Avenue, Cleveland, OH 44106-7215, USA, e-mail: luck@fafnir.astr.cwru.edu
[5] Visiting Astronomer, Cerro Tololo Inter-American Observatory, National Optical Astronomy Observatories which are operated by the Association of Universities for Research in Astronomy, Inc., under contract with the US National Science Foundation
[6] Harvard-Smithsonian Center for Astrophysics, 60 Garden Street, MS 16, Cambridge, MA 02138, USA
e-mail: dbersier@cfa.harvard.edu
[7] Special Astrophysical Observatory, Russian Academy of Sciences, Nizhny Arkhyz, Stavropol Territory, 369167, Russia
e-mail: valenta@sao.ru; panchuk@sao.ru
[8] SAO RAS and Isaac Newton Institute of Chile, SAO RAS Branch, Russia
[9] EdIC group, Universidade de São Paulo, São Paulo, Brazil
e-mail: ueda@ime.usp.be

Received 31 July 2001 / Accepted 10 October 2001

Abstract. A number of studies of abundance gradients in the galactic disk have been performed in recent years. The results obtained are rather disparate: from no detectable gradient to a rather significant slope of about -0.1 dex kpc^{-1}. The present study concerns the abundance gradient based on the spectroscopic analysis of a sample of classical Cepheids. These stars enable one to obtain reliable abundances of a variety of chemical elements. Additionally, they have well determined distances which allow an accurate determination of abundance distributions in the galactic disc. Using 236 high resolution spectra of 77 galactic Cepheids, the radial elemental distribution in the galactic disc between galactocentric distances in the range 6–11 kpc has been investigated. Gradients for 25 chemical elements (from carbon to gadolinium) are derived. The following results were obtained in this study. Almost all investigated elements show rather flat abundance distributions in the middle part of galactic disc. Typical values for iron-group elements lie within an interval from ≈-0.02 to ≈-0.04 dex kpc^{-1} (in particular, for iron we obtained $\mathrm{d[Fe/H]}/\mathrm{d}R_\mathrm{G} = -0.029$ dex kpc^{-1}). Similar gradients were also obtained for O, Mg, Al, Si, and Ca. For sulphur we have found a steeper gradient (-0.05 dex kpc^{-1}). For elements from Zr to Gd we obtained (within the error bars) a near to zero gradient value. This result is reported for the first time. Those elements whose abundance is not expected to be altered during the early stellar evolution (e.g. the iron-group elements) show at the solar galactocentric distance [El/H] values which are essentially solar. Therefore, there is no apparent reason to consider our Sun as a metal-rich star. The gradient values obtained in the present study indicate that the radial abundance distribution within 6–11 kpc is quite homogeneous, and this result favors a galactic model including a bar structure which may induce radial flows in the disc, and thus may be responsible for abundance homogenization.

Key words. stars: abundances – stars: supergiants – galaxy: abundances – galaxy: evolution

Send offprint requests to: S. M. Andrievsky,
e-mail: scan@deneb.odessa.ua

⋆ Based on spectra collected at McDonald – USA, SAORAS – Russia, KPNO – USA, CTIO – Chile, MSO – Australia, OHP – France.

⋆⋆ Full Table 1 is only available in electronic form at http://www.edpsciences.org

Table A1 (Appendix) is only, and Table 2 also, available in electronic form at the CDS via anonymous ftp to cdsarc.u-strasbg.fr (130.79.128.5)
or via
http://cdsweb.u-strasbg.fr/cgi-bin/qcat?J/A+A/381/32

1. Introduction

In recent years the problem of radial abundance gradients in spiral galaxies has emerged as a central problem in the field of galactic chemodynamics. Abundance gradients as observational characteristics of the galactic disc are among the most important input parameters in any theory of galactic chemical evolution. Further development of theories of galactic chemodynamics is dramatically hampered by the scarcity of observational data, their large uncertainties and, in some cases, apparent contradictions between independent observational results. Many questions concerning the present-day abundance distribution in the galactic disc, its spatial properties, and evolution with time, still have to be answered.

Discussions of the galactic abundance gradient, as determined from several studies, were provided by Friel (1995), Gummersbach et al. (1998), Hou et al. (2000). Here we only briefly summarize some of the more pertinent results.

1) A variety of objects (planetary nebulae, cool giants/supergiants, F-G dwarfs, old open clusters) seem to give evidence that an abundance gradient exists. Using DDO, Washington, *UBV* photometry and moderate resolution spectroscopy combined with metallicity calibrations for open clusters and cool giants the following gradients were derived ($\mathrm{d[Fe/H]}/\mathrm{d}R_\mathrm{G}$): -0.05 dex kpc^{-1} (Janes 1979), -0.095 dex kpc^{-1} (Panagia & Tosi 1981), -0.07 dex kpc^{-1} (Harris 1981), -0.11 dex kpc^{-1} (Cameron 1985), -0.017 dex kpc^{-1} (Neese & Yoss 1988), -0.13 dex kpc^{-1} (Geisler et al. 1992), -0.097 dex kpc^{-1} (Thogersen et al. 1993), -0.09 dex kpc^{-1} (Friel & Janes 1993), -0.091 dex kpc^{-1} (Friel 1995), -0.09 dex kpc^{-1} (Carraro et al. 1998), -0.06 dex kpc^{-1} (Friel 1999; Phelps 2000). One must also add that there have been attempts to derive the abundance gradient (specifically $\mathrm{d[Fe/H]}/\mathrm{d}R_\mathrm{G}$) using high-resolution spectroscopy of cool giant and supergiant stars. Harris & Pilachowski (1984) obtained -0.07 dex kpc^{-1}, while Luck (1982) found a steeper gradient of -0.13 dex kpc^{-1}.

Oxygen and sulphur gradients determined from observations of planetary nebulae are -0.058 dex kpc^{-1} and -0.077 dex kpc^{-1} respectively (Maciel & Quireza 1999), with slightly flatter values for neon and argon, as in Maciel & Köppen (1994). A smaller slope was found in an earlier study of Pasquali & Perinotto (1993). According to those authors the nitrogen abundance gradient is -0.052 dex kpc^{-1}, while that of oxygen is -0.030 dex kpc^{-1}.

2) From young B main sequence stars, Smartt & Rolleston (1997) found a gradient of -0.07 dex kpc^{-1}, while Gehren et al. (1985), Fitzsimmons et al. (1992), Kaufer et al. (1994) and Kilian-Montenbruck et al. (1994) derived significantly smaller values: -0.03–0.00 dex kpc^{-1}. No systematic abundance variation with galactocentric distance was found by Fitzsimmons et al. (1990). The recent studies of Gummersbach et al. (1998) and Rolleston et al. (2000) support the existence of a gradient (-0.07 dex kpc^{-1}). The elements in these studies were C-N-O and Mg-Al-Si.

3) Studies of the abundance gradient (primarily nitrogen, oxygen, sulphur) in the Galactic disc based on young objects such as H II regions give positive results: either significant slopes from -0.07 to -0.11 dex kpc^{-1} according to: Shaver et al. (1983) for nitrogen and oxygen, Simpson et al. (1995) for nitrogen and sulphur, Afflerbach et al. (1997) for nitrogen, Rudolph et al. (1997) for nitrogen and sulphur, or intermediate gradients of about -0.05 to -0.06 dex kpc^{-1} according to: Simpson & Rubin (1990) for sulphur, Afflerbach et al. (1997) for oxygen and sulphur; and negative ones: weak or nonexistent gradients as concluded by Fich & Silkey (1991); Vilchez & Esteban (1996), Rodriguez (1999). Recently Peña et al. (2000) derived oxygen abundances in several H II regions and found a rather flat distribution with galactocentric distance (coefficient -0.04 dex kpc^{-1}). The same results were also reported by Deharveng et al. (2000).

As one can see, there is no conclusive argument allowing one to come to a definite conclusion about whether or not a significant abundance gradient exists in the galactic disc, at least for all elements considered and within the whole observed interval of galactocentric distances. Compared to other objects supplying us with an information about the radial distribution of elemental abundances in the galactic disc, Cepheids have several advantages:

1) they are primary distance calibrators which provide excellent distance estimates;
2) they are luminous stars allowing one to probe to large distances;
3) the abundances of many chemical elements can be measured from Cepheid spectra (many more than from H II regions or B stars). This is important for investigation of the distribution in the galactic disc of absolute abundances and abundance ratios. Additionally, Cepheids allow the study of abundances past the iron-peak which are not generally available in H II regions or B stars;
4) lines in Cepheid spectra are sharp and well-defined which enables one to derive elemental abundances with high reliability.

In view of the inconsistencies in the current results on the galactic abundance gradient, and those advantages which are afforded by Cepheids, we have undertaken a large survey of Cepheids in order to provide independent information which should be useful as boundary conditions for theories of galactic chemodynamics. We also hope that the results on the abundance gradient from the Cepheids will also be helpful to constrain the structure and age of the bar, and its influence on the metallicity gradient. This first paper in this series on abundance gradients from Cepheids presents the results for the solar neighbourhood.

2. Observations

For the great majority of the program stars multiphase observations were obtained. From the total number of the spectra for each star we selected those showing no or at most a small asymmetry of the spectral lines. For the distant (fainter) Cepheids we have analyzed 3–4 spectra in order to derive the abundances, while for the nearby stars 2–3 spectra were used. This is predicated on the fact that the brighter stars have higher S/N spectra and thus better determined equivalent widths. For some stars we have only one spectrum, and for a few Cepheids more than four spectra were analyzed.

Information about the program stars and spectra is given in Table 1. Note that we also added to our sample two distant Cepheids (TV Cam and YZ Aur) which were previously analyzed by Harris & Pilachowski (1984). We have used their data for these stars but atmospheric parameters and elemental abundances (specifically the iron content) were re-determined using the same methodology as for other program stars (see next section).

3. Methodology

3.1. Line equivalent widths

The line equivalent widths in the Cepheid spectra were measured using the Gaussian approximation, or in some cases, by direct integration. To estimate the internal accuracy of the measurements we have compared the equivalent widths of lines present in adjacent overlapping échelle orders. In no case did the difference between independent estimates exceed 10%. The measured equivalent widths were analyzed in the LTE approximation using the WIDTH9 code of Kurucz. Only lines having $W_\lambda \leq 165$ mÅ were used for abundance determination. The total number of lines used in the analysis exceeds 41 000.

3.2. Atmosphere models

Plane-parallel LTE atmosphere models (ATLAS9) from Kurucz (1992) were used to determine the elemental abundances. Final models were interpolated (in $T_{\rm eff}$ and $\log g$) from the solar metallicity grid computed using a microturbulent velocity of 4 km s^{-1}. The adopted microturbulent velocities vary from 3 to 8 km s^{-1} but numerical experiment shows that the derived abundances are not substantially altered by the mismatch between the model microturbulence and the value used to compute the abundances. Note that the ATLAS9 models are in a regime where the convection problem discovered by Castelli (1996) does not cause a significant problem.

3.3. Oscillator strengths and damping constants

The oscillator strengths used in present study were obtained through an inverted solar analysis (with elemental abundances adopted following Grevesse et al. 1996). They were derived using selected unblended solar lines from the solar spectrum by Kurucz et al. (1984). A detailed description and list of the $\log gf$ values can be found in Kovtyukh & Andrievsky (1999). The damping constants for the lines of interest were taken from the list of B. Bell. It is well known that the classical treatment of the van der Waals broadening leads to broadening coefficients which are too small (see Barklem et al. 2000).

3.4. Stellar parameters

The effective temperature for each program star was determined using the method described in detail in Kovtyukh & Gorlova (2000). That method is based on the use of relations between effective temperature and the line depth ratios (each ratio is for the weak lines with different excitation potentials of the same chemical element). The advantages of this method are the following: such ratios are sensitive to the temperature variations, they do not depend upon the abundances and interstellar reddening. The main source of initial temperatures used for the calibrating relations was Fry & Carney (1997). Their data are in good agreement with the results obtained by other methods, such as the infrared flux method (Fernley et al. 1989) or detailed analysis of energy distribution (Evans & Teays 1996). Another source was photometry (Kiss 1998).

The number of temperature indicators (ratios) is typically 30. The precision of the $T_{\rm eff}$ determination is 10–30 K (standard error of the mean) from the spectra with S/N greater than 100, and 30–50 K for S/N less than 100. Although an internal error of $T_{\rm eff}$ determination appears to be small, a systematic shift of the zero-point of $T_{\rm eff}$ scale may exist. Nevertheless, an uncertainty in the zero-point (if it exists) can affect absolute abundances in each program star, but the slopes of the abundance distributions should be hardly affected.

The microturbulent velocity and gravity were found using the technique put forth by Kovtyukh & Andrievsky (1999). This method was applied to an investigation of LMC F supergiants with well known distances, and it produced much more appropriate gravities for those stars than were previously determined (see Hill et al. 1995). The method also allowed to solve several problems connected with abundances in the Magellanic Cloud supergiants (for details see Andrievsky et al. 2001). Results on $T_{\rm eff}$, $\log g$ and $V_{\rm t}$ determination are gathered in Table 1 (the quoted precision of the $T_{\rm eff}$ values presented in Table 1 is not representative of the true precision which is stated above).

Several remarks on the gravity results for our program Cepheids have to be made. It is expected that the gravities of Cepheids, being averaged over the pulsational cycle, should correlate with their pulsational periods in the sense that lower gravities correspond to larger periods. As it was analytically shown by Gough et al. (1965), the pulsational period P behaves as $P \sim R^2 M^{-1}$, i.e. $\sim g^{-1}$ (where R, M and g are the radius, mass and gravity of a Cepheid

Table 1. Program Cepheids, their spectra and results for individual phases.

Star	P, d	JD, 24+	ϕ	Telescope	$T_{\rm eff}$, K	$\log g$	$V_{\rm t}$, km s^{-1}	[Fe/H]
V473 Lyr (s)	1.4908	49906.43160	0.793	OHP 1.93 m	6163	2.45	4.20	–0.09
		49907.57360	0.559	OHP 1.93 m	6113	2.60	4.50	–0.05
SU Cas(s)	1.9493	50674.95633	0.902	MDO 2.1 m	6594	2.60	3.85	–0.02
		50675.96550	0.420	MDO 2.1 m	6162	2.25	3.00	–0.00
		50678.93059	0.941	MDO 2.1 m	6603	2.50	3.50	–0.01
		51473.79052	0.704	MDO 2.1 m	6201	2.30	2.85	–0.00
EU Tau (s)	2.1025	51096.90943	0.172	MDO 2.1 m	6203	2.00	3.00	–0.09
		51097.89587	0.641	MDO 2.1 m	6014	2.20	3.30	–0.03
IR Cep (s)	2.1140	48821.46940	0.137	SAORAS 6 m	6162	2.40	4.10	+0.00

respectively). A similar relation between pulsational period and gravity can be also derived, for example, by combining observational "period-mass" and "period-radius" relations established for Cepheids by Turner (1996) and Gieren et al. (1998) respectively.

As for each star of our sample we have only a limited number of the gravity estimates, in Fig. 1 we simply plotted individual $\log g$ (gravity in cm s^{-2}) values for a given Cepheid versus its pulsational period of the fundamental mode (period is given in days). The general trend can be clearly traced from this figure. For the long-period Cepheids the scatter in the gravities derived at the different pulsational phases achieves approximately 1 dex. The instantaneous gravity value, in fact, is a combination of the static component GM/R^2 and dynamical term $\gamma\ {\rm d}V/{\rm d}t$ (γ is the projection factor and V is the radial velocity). This means that observed amplitudes of the gravity variation do not reflect purely pulsational changes of the Cepheid radius. Nevertheless, there may exist some additional mechanism artificially "lowering" gravities which are derived through spectroscopic analysis, and thus increasing an amplitude of the gravity variation. Such effects as, for example, sphericity of the Cepheid atmospheres, additional UV flux and connected with it an overionization of some elements, stellar winds and mass loss, rotation and macroturbulence, may contribute to some increase of the spectroscopic gravity variation over a pulsational cycle. It is quite likely that these effects should be more pronounced in the more luminous (long-period) Cepheids, and they may affect the abundances resulting from the gravity sensitive ionized species. To investigate this problem one needs to perform a special detailed multiphase analysis for Cepheids with various pulsational periods. From our sample of stars only for TU Cas, U Sgr and SV Vul we have enough data to observe effects.

In Figs. 2–3 we plotted Ce and Eu abundances together with spectroscopic gravities versus pulsational phases for the intermediate-period Cepheid U Sgr ($P \approx 7$ days) and for SV Vul ($P \approx 45$ days), one of the longest period Cepheid among our program stars. A scatter of about 0.15 dex is seen for both elements which are presented in the spectra only by ionized species. Inspecting Fig. 3 one might suspect some small decrease of abundances around phase 0.4 (roughly corresponds to a maximum in SV Vul radius). It can be attributed to NLTE effects, which should increase in the extended spherical atmosphere of lower density. More precisely, a small decrease in the abundances may be caused by additional overionization of the discussed ions having rather low ionization potentials (about 11 eV). Although the *s*-process elements in Cepheids are measured primarily by ionized species, and any errors in the stellar gravities at some phases propagate directly into the abundance results, we do not think that this effect may have some radical systematic influence on abundance results for the *s*-process elements in our program stars. The reasons are the following. An indicated decrease in the abundance is rather small, even for the long-period Cepheid, and practically is not seen for shorter periods. In fact, a decrease of about 0.15 dex is comparable with errors in the abundance determination for the elements with small number of lines, like *s*-process elements. One can also add that the abundances averaged from different phases should be sensitive to this effect even to a lesser extent.

4. Elemental abundances

Detailed abundance results are presented in the Appendix (Table A1) and Table 2. The Appendix contains the per species abundances averaged over all individual spectra (phases) for each star along with the total number of lines and standard deviation. Table 2 contains the final averaged abundance per element. The latter abundances were obtained by averaging all lines from all ions at all phases: that is, for example a sum of all iron line abundances from all phases and divide by the total number of lines. The iron abundance for individual phases is presented in Table 1, and the mean iron abundance for each star is also repeated in Table 3. Note that standard deviation of the abundance of an element falls within the range 0.05–0.20 dex for all determinations. Because the number of lines used for some elements is large (especially for iron), the standard error of the mean abundance is very small.

Note that the modified method of LTE spectroscopic analysis described in Kovtyukh & Andrievsky (1999) specifies the microturbulent velocity as a fitting parameter to avoid any systematic trend in the "[Fe/H]$-EW$" relation based on Fe II lines (which are not significantly affected by NLTE effects unlike Fe I lines which may be adversely affected). With the microturbulent velocity obtained in this way, the Fe I lines demonstrate a progressively decreasing iron abundance as a function of increasing equivalent

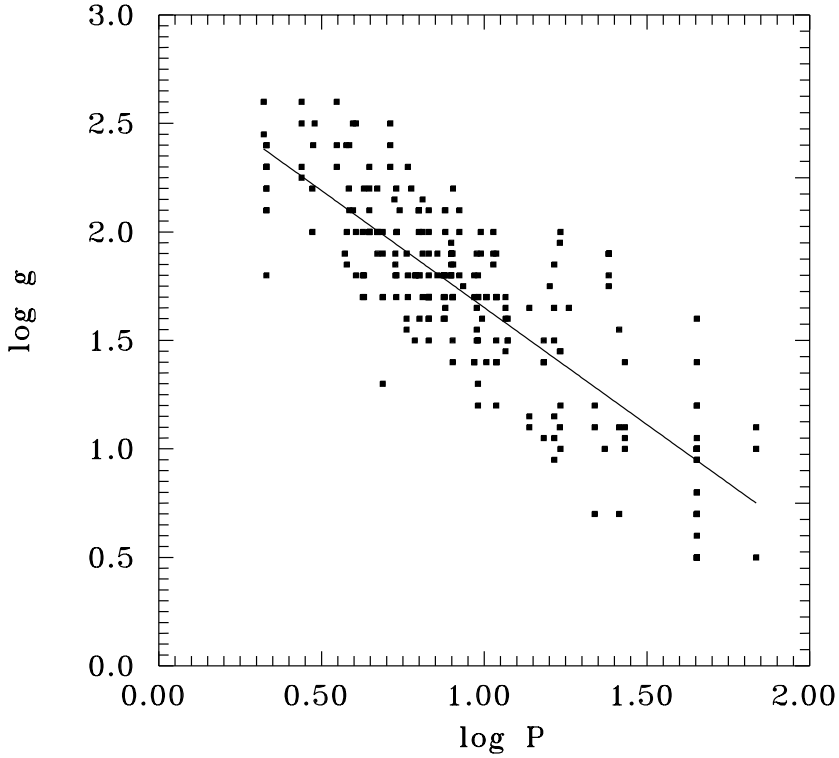

Fig. 1. Program Cepheid gravities vs. their pulsational periods.

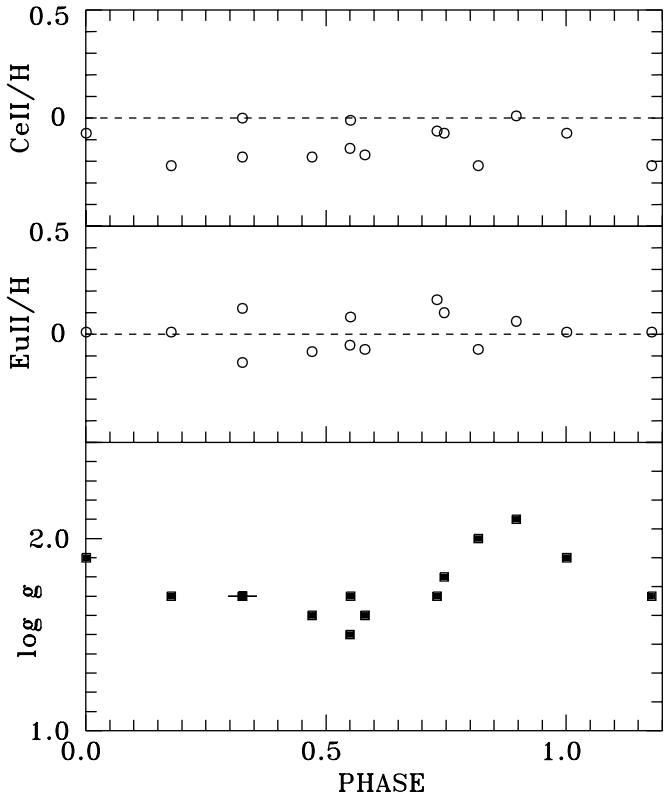

Fig. 2. Relative-to-solar Ce and Eu abundance and spectroscopic gravity of U Sgr vs. its pulsational phases.

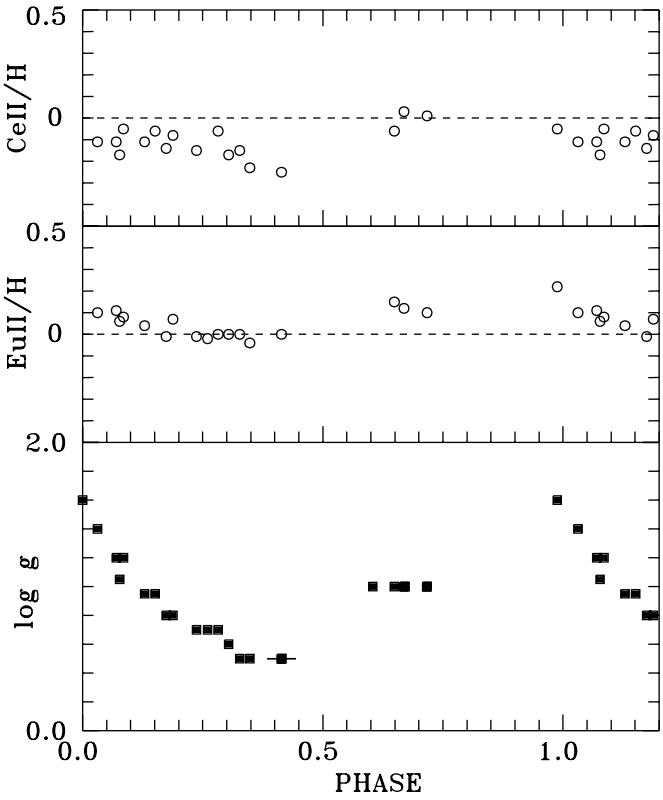

Fig. 3. Same as Fig. 2 but for SV Vul.

width. Kovtyukh & Andrievsky (1999) attribute this behavior to departures from LTE in Fe I. To determine the true iron abundance from Fe I lines one refers the abundance to the lowest EW, and it is therefore determined using the [Fe/H]$-EW$ relation for these lines (and this

Table 2. Averaged relative-to-solar elemental abundance for program Cepheids.

Star	C	O	Na	Mg	Al	Si	S	Ca	Sc	Ti	V	Cr	Mn
V473 Lyr (s)	−0.34	−0.24	0.01	−0.14	−0.06	−0.03	0.09	−0.10	−0.05	−0.06	−0.04	−0.08	−0.22
SU Cas (s)	−0.24	−0.02	0.20	−0.24	0.05	0.07	0.11	−0.01	−0.13	0.13	0.08	0.12	0.07
EU Tau (s)	−0.24	−0.05	0.24	−0.28	−0.01	0.04	0.09	−0.05	−0.07	0.03	−0.05	−0.02	−0.05
IR Cep (s)	−0.04	–	0.28	−0.39	0.12	0.17	0.34	−0.06	−0.03	0.09	0.26	−0.12	−0.02
TU Cas	−0.19	−0.03	0.15	−0.19	0.14	0.10	−0.03	−0.02	−0.19	0.05	0.02	0.02	0.06
DT Cyg (s)	−0.12	0.01	0.33	0.04	0.17	0.12	0.15	0.05	−0.01	0.21	0.14	0.18	0.19
V526 Mon (s)	−0.28	−0.52	0.11	−0.09	–	−0.01	0.05	−0.08	−0.20	−0.04	−0.18	−0.02	−0.14
V351 Cep (s)	−0.19	−0.09	0.17	−0.30	−0.03	0.07	0.26	−0.10	0.01	0.08	0.08	0.03	−0.03
VX Pup	–	–	0.08	–	–	−0.06	–	−0.33	−0.13	−0.01	−0.02	−0.16	−0.10
SZ Tau (s)	−0.20	−0.02	0.25	–	0.14	0.07	0.19	0.02	0.02	0.06	0.10	0.18	0.09
V1334 Cyg (s)	−0.30	−0.23	0.18	−0.31	0.15	0.08	0.11	−0.03	−0.01	0.02	−0.01	−0.03	0.03
BG Cru (s)	−0.18	0.08	0.24	–	0.29	0.07	–	−0.01	−0.33	0.13	0.15	−0.04	−0.01
BD Cas (s)	−0.14	−0.09	−0.03	−0.26	−0.09	0.03	0.26	−0.19	−0.23	−0.06	−0.06	−0.14	−0.13
RT Aur	−0.22	−0.01	0.29	−0.14	0.13	0.12	0.19	0.09	0.05	0.10	0.05	0.08	0.11
DF Cas	−0.30	–	0.16	−0.33	–	0.03	0.39	−0.18	−0.09	0.00	−0.01	0.11	−0.12
SU Cyg	−0.21	−0.25	0.23	−0.16	0.17	0.04	0.02	0.01	−0.11	0.01	0.06	0.02	0.02
ST Tau	−0.27	−0.29	0.23	−0.18	0.03	0.03	0.04	−0.04	−0.11	0.10	−0.07	−0.04	−0.02
V1726 Cyg (s)	−0.22	–	0.29	−0.12	0.07	0.11	0.17	−0.16	−0.05	0.15	–	−0.07	0.00
BQ Ser	−0.15	−0.13	0.12	−0.14	0.14	0.07	0.13	−0.05	−0.17	0.03	−0.01	0.04	−0.04
Y Lac	−0.26	−0.37	0.13	−0.24	0.13	0.03	−0.04	−0.05	−0.26	−0.03	0.02	−0.07	−0.09
T Vul	−0.26	0.00	0.13	−0.31	0.12	0.04	0.12	0.03	−0.19	0.00	0.00	0.10	0.01
FF Aql (s)	−0.31	−0.23	0.25	−0.24	0.12	–	0.01	−0.03	−0.11	0.09	0.14	0.06	0.04
CF Cas	−0.19	0.06	0.09	−0.21	0.10	0.01	0.10	−0.01	−0.04	−0.00	−0.06	0.06	−0.01
BG Lac	−0.17	0.10	0.17	−0.25	0.08	0.04	0.09	−0.01	−0.11	0.03	−0.05	0.06	0.04
Del Cep	−0.17	0.01	0.20	−0.16	0.16	0.10	0.15	0.01	0.01	0.04	0.09	0.06	0.17
V1162 Aql (s)	−0.14	−0.19	0.13	−0.19	0.13	0.06	–	−0.03	−0.21	−0.03	−0.02	0.02	−0.01
CV Mon	−0.25	0.02	0.03	−0.32	−0.05	0.01	0.08	−0.19	−0.14	0.10	0.30	0.04	−0.05
V Cen	−0.17	0.02	0.01	–	0.11	0.03	0.14	−0.03	0.00	0.09	0.03	−0.04	−0.11
V924 Cyg (s:)	−0.30	–	−0.04	−0.38	0.09	−0.04	0.05	−0.21	−0.37	−0.21	0.01	−0.09	0.10
MY Pup (s)	−0.36	−0.12	0.14	−0.36	0.03	−0.08	−0.14	−0.13	−0.17	−0.09	−0.09	−0.18	−0.24
Y Sgr	−0.14	−0.06	0.22	−0.03	0.27	0.12	0.17	0.04	−0.24	0.01	0.07	0.17	0.11
EW Sct	−0.07	−0.04	0.07	−0.10	0.15	0.08	0.15	−0.01	−0.09	0.09	0.08	0.05	0.08
FM Aql	−0.24	−0.19	0.32	0.00	0.33	0.17	0.24	0.17	−0.17	0.15	0.10	0.19	0.11
TX Del	0.06	0.16	0.48	−0.22	–	–	–	0.16	–	0.17	0.15	–	0.38
V367 Sct	−0.38	–	0.21	−0.48	0.21	0.05	0.15	−0.15	0.07	0.24	0.06	−0.05	−0.13
X Vul	−0.16	0.03	0.18	−0.20	0.17	0.08	0.20	−0.04	−0.09	0.08	0.04	0.12	0.08
AW Per	−0.23	−0.03	0.24	−0.27	0.07	0.06	0.18	−0.03	−0.15	0.01	0.15	0.27	0.10
U Sgr	−0.16	0.03	0.20	−0.17	0.22	0.07	0.15	0.03	−0.16	0.06	0.03	0.10	0.06
V496 Aql (s)	−0.20	−0.15	0.24	−0.12	0.10	0.11	0.13	−0.03	0.10	0.06	0.06	0.09	0.05
Eta Aql	−0.20	−0.10	0.19	−0.19	0.23	0.12	0.08	−0.02	−0.18	0.03	0.02	0.22	0.12
BB Her	−0.10	0.04	0.40	−0.01	0.23	0.15	–	−0.01	0.07	0.09	0.07	0.10	0.30
RS Ori	−0.45	−0.18	0.06	−0.30	0.02	0.02	0.00	−0.06	−0.19	0.11	−0.12	−0.09	−-0.11
V440 Per (s)	−0.34	−0.21	0.05	−0.33	0.06	0.00	−0.06	−0.16	−0.14	0.05	0.00	−0.06	−0.04
W Sgr	−0.25	0.02	0.18	−0.25	−0.01	0.04	0.11	−0.01	−0.12	0.03	0.03	0.03	0.03
RX Cam	−0.25	−0.11	0.18	−0.23	0.06	0.05	0.04	−0.05	0.04	0.10	0.03	0.08	0.02
W	−0.27	−0.12	0.18	−0.28	0.10	0.03	0.05	−0.08	0.05	0.09	0.00	−0.02	−0.02
U Vul	−0.18	−0.03	0.18	−0.16	0.12	0.09	0.17	−0.05	−0.28	0.05	0.02	0.10	0.01
DL Cas	−0.31	−0.01	0.11	0.11	0.14	0.02	0.21	0.01	−0.16	0.03	−0.04	0.10	0.07
AC Mon	−0.42	–	0.24	−0.40	–	−0.02	−0.15	−0.10	−0.07	0.12	–	−0.08	−0.19
V636 Cas (s)	−0.17	−0.09	0.29	−0.07	0.09	0.08	0.12	0.15	0.25	0.05	0.05	0.30	0.10
S Sge	−0.12	0.04	0.24	−0.22	0.14	0.16	0.17	0.03	0.27	0.12	0.17	0.22	0.19
GQ Ori	−0.37	−0.12	0.17	0.11	0.04	0.00	0.04	−0.25	–	0.06	0.04	0.01	−0.14
V500 Sco	−0.20	−0.13	0.13	−0.23	0.08	0.02	0.06	−0.09	−0.13	−0.06	−0.10	−0.07	−0.03
FN Aql	−1.31	−0.08	0.19	−0.21	0.10	0.00	−0.02	−0.07	−0.07	0.04	0.01	−0.04	−0.12
YZ Sgr	−0.07	−0.07	0.31	−0.22	0.18	0.12	0.18	0.00	–	0.03	0.03	0.09	0.07
S Nor	−0.23	−0.19	0.27	−0.24	0.16	0.05	0.10	−0.03	0.01	0.05	0.02	−0.08	−0.10
Beta Dor	−0.31	−0.08	0.07	−0.30	0.07	0.00	−0.04	−0.18	−0.11	0.01	−0.05	−0.04	0.03
Zeta Gem	−0.24	−0.12	0.25	−0.15	0.07	0.04	0.03	−0.06	0.13	0.06	0.02	0.00	0.05
Z Lac	−0.32	−0.10	0.23	−0.23	0.07	0.05	0.14	0.04	−0.18	0.07	−0.02	0.05	0.05
VX Per	−0.25	−0.15	0.15	−0.31	0.03	0.00	0.04	−0.12	−0.05	−0.03	−0.11	−0.06	−0.09
V340 Nor(s:)	−0.08	0.07	0.29	−0.30	0.00	0.03	0.18	−0.16	−0.12	0.00	−0.07	0.01	−0.03
RX Aur	−0.29	−0.02	0.18	−0.20	0.04	0.05	−0.01	−0.09	−0.31	0.05	−0.07	0.04	0.08
TT Aql	−0.09	0.13	0.28	−0.19	0.20	0.11	0.33	0.08	0.12	0.04	−0.01	0.09	0.14
SV Mon	−0.84	−0.28	0.28	−0.16	0.10	0.00	−0.10	−0.09	−0.30	−0.06	−0.16	−0.07	−0.16
X Cyg	−0.29	0.05	0.26	−0.09	0.18	0.13	0.13	0.04	–	0.21	0.11	0.23	0.11
RW Cam	−0.14	−0.05	0.19	−0.23	0.12	0.07	0.18	0.02	0.12	0.04	−0.02	0.06	0.05
CD Cyg	−0.18	−0.11	0.23	−0.37	0.19	0.09	0.28	0.08	0.03	0.08	0.06	0.05	0.10
Y Oph (s)	−0.14	−0.01	0.12	−0.31	0.14	0.03	0.15	−0.15	0.33	0.06	0.05	0.03	0.04
SZ Aql	−0.01	−0.04	0.28	−0.12	0.28	0.17	0.24	0.14	0.11	0.14	0.12	0.19	0.20
WZ Sgr	0.03	0.13	0.39	0.01	0.28	0.28	0.51	0.19	0.12	0.23	0.17	0.19	0.15
SW Vel	−0.13	0.18	0.17	0.16	0.04	−0.03	0.17	−0.16	0.08	−0.06	−0.14	0.14	−0.12
X Pup	−0.29	−0.11	0.18	–	0.10	−0.05	0.02	0.06	−0.18	−0.08	−0.16	−0.07	0.07
T Mon	−0.27	0.08	0.35	–	0.10	0.13	–	0.09	–	0.06	0.03	0.27	0.14
SV Vul	0.02	−0.01	0.04	−0.10	0.13	0.06	0.16	−0.04	–	0.02	−0.08	0.02	−0.02
S Vul	−0.34	−0.40	0.21	–	0.22	−0.03	0.22	−0.04	–	0.03	0.04	0.10	−0.06

resulting iron abundance from Fe I lines should be equal to the mean abundance from Fe II provided the surface gravity was properly chosen).

Ni I has the second largest number of weak and intermediate strength lines (after Fe) in almost all program spectra. Ni I has an atomic structure similar to that of Fe I. Therefore, one can suppose that in many respects it should react to departures from LTE in much the same way as neutral iron. Thus, to estimate the true nickel content from Ni I lines (lines of ionized nickel are not available), we have applied the same method used for Fe I lines adopting for the microturbulent velocity the value determined from Fe II; i.e., we have extrapolated the [Ni/H]$-EW$ relation back to the lowest EW and adopted the intercept abundance as indicative of the true abundance.

Manganese is an important element, but in the available spectral interval it is represented, as a rule, by only three Mn I lines with intermediate equivalent widths.

Table 2. continued.

Star	Fe	Co	Ni	Cu	Zn	Y	Zr	La	Ce	Nd	Eu	Gd
V473 Lyr (s)	−0.06	−0.13	−0.11	−0.10	0.12	0.10	0.02	0.20	0.11	0.03	−0.02	0.00
SU Cas (s)	−0.01	−0.19	0.00	0.34	0.18	0.19	0.02	0.21	−0.04	0.12	0.02	−0.20
EU Tau (s)	−0.06	−0.02	−0.08	0.21	–	0.07	−0.08	0.16	−0.18	−0.02	0.01	0.18
IR Cep (s)	−0.01	−0.20	−0.07	−0.47	–	0.03	0.16	–	0.05	−0.11	–	–
TU Cas	0.03	−0.08	−0.04	0.15	0.46	0.17	0.01	0.24	−0.05	0.08	0.11	0.17
DT Cyg (s)	0.11	0.23	0.14	0.42	0.20	0.46	−0.06	0.21	0.01	0.25	0.20	0.33
V526 Mon (s)	−0.13	0.04	−0.07	–	–	–	−0.11	0.41	–	0.25	0.16	–
V351 Cep (s)	0.03	−0.01	0.00	−0.05	0.14	0.19	−0.01	0.26	−0.10	0.12	–	0.16
VX Pup	−0.13	–	−0.18	0.25	–	0.10	–	–	–	0.35	−0.15	–
SZ Tau (s)	0.08	−0.01	0.02	–	0.39	0.17	−0.03	0.31	0.06	0.23	0.15	–
V1334 Cyg (s)	−0.04	−0.29	−0.10	0.39	–	0.18	−0.15	0.21	−0.17	0.13	0.13	–
BG Cru (s)	−0.02	−0.06	−0.16	−0.68	–	–0.04	−0.04	–	0.28	−0.14	0.25	–
BD Cas (s)	−0.07	0.09	−0.26	−0.14	–	0.01	0.13	0.41	0.19	−0.25	–	0.30
RT Aur	0.06	−0.09	0.05	0.15	0.24	0.24	−0.04	0.14	−0.17	0.07	0.01	0.01
DF Cas	0.13	−0.30	0.04	−0.43	–	0.06	0.22	–	0.07	0.38	0.28	–
SU Cyg	−0.00	−0.01	−0.11	0.15	–	0.16	0.01	0.27	−0.19	0.08	0.06	0.10
ST Tau	−0.05	−0.33	−0.04	0.19	0.02	0.18	−0.13	0.17	−0.10	0.14	0.04	0.13
V1726 Cyg (s)	−0.02	–	−0.15	–	–	0.14	–	–	–	0.24	0.31	–
BQ Ser	−0.04	−0.17	−0.07	0.08	0.35	0.13	−0.10	0.13	−0.09	0.22	0.07	0.20
Y Lac	−0.09	–	−0.15	0.18	–	0.12	−0.24	0.11	−0.35	0.16	0.00	–
T Vul	0.01	0.01	−0.02	0.25	0.30	0.13	−0.02	0.20	−0.03	0.14	0.08	−0.12
FF Aql (s)	0.02	−0.13	0.01	0.45	–	0.31	−0.11	0.25	−0.13	0.08	0.17	0.22
CF Cas	−0.01	−0.15	−0.03	−0.11	0.25	0.11	−0.19	0.14	−0.17	0.04	0.06	−0.02
BG Lac	−0.01	−0.13	−0.03	0.10	0.28	0.14	−0.12	0.07	−0.17	0.05	0.02	0.18
Del Cep	0.06	−0.02	0.01	0.55	0.36	0.27	−0.14	0.25	−0.08	0.17	0.02	–
V1162 Aql (s)	0.01	−0.15	−0.02	0.28	0.14	0.21	−0.21	0.09	−0.24	0.02	−0.06	−0.23
CV Mon	−0.03	–	−0.08	−0.05	–	0.01	0.00	0.19	−0.03	0.29	0.13	–
V Cen	0.04	−0.21	0.11	0.16	0.37	0.35	0.18	0.26	0.02	0.28	0.20	–
V924 Cyg (s:)	−0.09	–	−0.14	0.12	–	−0.18	–	–	–	0.04	–	–
MY Pup (s)	−0.12	−0.10	−0.04	−0.25	−0.09	−0.03	−0.16	0.17	−0.10	−0.07	−0.04	–
Y Sgr	0.06	−0.07	0.03	–	0.38	0.31	−0.08	0.13	−0.15	0.10	−0.03	0.00
EW Sct	0.04	−0.10	−0.01	0.11	0.34	0.22	−0.12	0.29	−0.07	0.17	0.06	–
FM Aql	0.08	0.02	0.09	0.26	–	0.16	−0.01	0.23	−0.17	0.14	0.09	–
TX Del	0.24	–	0.17	–	–	0.07	–	0.13	−0.34	−0.38	–	–
V367 Sct	−0.01	0.03	−0.01	−0.02	–	−0.06	−0.15	0.45	–	0.18	0.36	–
X Vul	0.08	−0.11	0.07	0.07	0.35	0.23	−0.11	0.15	−0.15	0.10	0.03	0.04
AW Per	0.01	−0.01	0.04	0.57	0.51	0.11	−0.02	0.25	−0.11	0.10	0.11	−0.12
U Sgr	0.04	−0.12	0.01	0.02	0.24	0.22	−0.11	0.14	−0.12	0.05	0.01	−0.03
V496 Aql (s)	0.05	−0.09	0.03	–	0.33	0.14	−0.10	0.09	−0.23	0.02	−0.01	−0.09
Eta Aql	0.05	−0.27	0.04	0.28	0.14	0.23	−0.14	0.26	−0.19	0.10	0.04	−0.05
BB Her	0.15	−0.04	0.15	0.19	0.39	0.32	0.00	0.11	−0.17	0.02	0.08	–
RS Ori	−0.10	−0.01	−0.13	0.12	0.21	0.16	−0.12	0.18	−0.20	0.04	0.00	0.07
V440 Per (s)	−0.05	−0.13	−0.05	0.16	0.06	0.26	−0.13	0.30	−0.10	0.14	0.14	0.12
W Sgr	−0.01	−0.08	−0.04	0.21	0.22	0.20	−0.11	0.23	−0.07	0.06	−0.01	0.11
RX Cam	0.03	−0.14	0.03	0.20	0.14	0.23	−0.06	0.27	−0.17	0.10	0.09	0.15
W Gem	−0.04	−0.21	−0.07	0.11	0.16	0.23	−0.09	0.28	−0.10	0.15	0.10	0.07
U Vul	0.05	−0.09	0.05	0.13	0.31	0.21	−0.10	0.13	−0.06	0.13	0.02	0.02
DL Cas	−0.01	−0.04	0.00	−0.19	0.47	0.21	0.16	0.12	0.09	0.12	0.11	−0.05
AC Mon	−0.07	–	−0.11	−0.61	–	0.05	–	0.39	–	0.35	0.28	–
V636 Cas (s)	0.06	−0.09	0.09	−0.07	0.30	0.18	−0.11	0.16	−0.11	0.12	0.02	0.06
S Sge	0.10	0.00	0.12	0.26	0.39	0.28	0.02	0.29	−0.09	0.13	0.15	0.02
GQ Ori	−0.03	−0.01	−0.15	–	–	0.29	–	0.25	–	−0.16	0.09	–
V500 Sco	−0.02	−0.18	−0.06	−0.02	0.21	0.19	−0.19	0.18	−0.10	0.08	0.03	−0.24
FN Aql	−0.02	−0.14	−0.05	0.09	0.15	0.16	−0.07	0.23	−0.09	0.12	0.08	0.12
YZ Sgr	0.05	−0.06	0.03	0.11	0.22	0.35	−0.09	0.14	−0.10	0.01	0.02	−0.01
S Nor	0.05	−0.10	−0.07	−0.17	–	0.11	0.14	0.35	−0.10	0.00	0.02	–
Beta Dor	−0.01	−0.19	−0.04	−0.45	0.14	0.02	0.03	0.18	0.05	−0.05	0.04	0.20
Zeta Gem	0.04	−0.10	0.02	0.03	0.17	0.19	−0.07	0.21	−0.13	0.08	0.06	−0.06
Z Lac	0.01	−0.13	−0.02	0.14	0.25	0.20	−0.07	0.26	−0.04	0.12	0.06	0.09
VX Per	−0.05	−0.20	−0.10	0.05	0.18	0.16	−0.12	0.21	−0.13	0.08	0.03	0.00
V340 Nor(s:)	0.00	−0.13	0.01	−0.06	–	0.07	–	0.13	−0.25	−0.11	−0.06	0.12
RX Aur	−0.07	−0.15	−0.07	0.28	0.30	0.09	−0.11	0.28	−0.21	0.08	0.10	0.12
TT Aql	0.11	−0.07	0.08	0.05	0.41	0.28	−0.06	0.20	−0.09	0.14	0.05	0.01
SV Mon	−0.03	−0.28	−0.12	−0.07	0.16	0.26	−0.08	0.25	−0.14	0.13	0.03	–
X Cyg	0.12	0.06	0.09	0.24	0.35	0.33	−0.03	0.29	0.02	0.15	0.14	0.14
RW Cam	0.04	−0.08	0.05	−0.08	0.45	0.17	−0.04	0.25	−0.11	0.10	0.06	0.02
CD Cyg	0.07	−0.03	0.05	0.01	0.32	0.31	−0.10	0.23	−0.07	0.17	0.08	0.10
Y Oph (s)	0.05	−0.05	0.03	0.07	0.14	0.33	−0.04	0.28	−0.07	0.21	0.13	0.08
SZ Aql	0.15	−0.02	0.03	0.05	0.42	–	0.04	0.21	−0.12	0.15	0.12	0.12
WZ Sgr	0.17	0.12	0.21	0.13	0.35	0.30	−0.08	0.24	−0.08	0.18	0.15	0.08
SW Vel	0.01	−0.25	−0.06	−0.41	0.30	0.21	–	0.23	0.00	0.22	0.16	0.10
X Pup	−0.03	−0.25	−0.08	−0.13	0.26	0.14	0.01	0.27	−0.09	0.22	0.09	−0.04
T Mon	0.13	−0.03	0.05	–	0.34	–	0.04	0.30	0.02	0.22	0.15	–
SV Vul	0.03	−0.13	0.00	−0.16	0.22	0.26	−0.08	0.20	−0.13	0.05	0.04	0.03
S Vul	−0.02	−0.22	0.02	0.03	–	0.22	−0.06	0.18	−0.25	0.15	0.02	−0.01

As for nickel, we suppose that the Mn I ion should be sensitive to departures from LTE at the same level as Fe I. Because of the lack of sufficient numbers of Mn I lines it is not possible to proceed in the same way as with Fe I lines. Therefore, to estimate the true manganese content from each spectrum, we used the corresponding dependencies between iron abundance from Fe I lines and their equivalent widths, and corrected the manganese abundance derived from the available Mn I lines. The abundance correction for a given equivalent width (EW) of Mn I line has been found as Δ[Mn/H] = Δ[Fe/H] = $a \times EW$ (where a is the linear coefficient in the [Fe/H]$-EW$ relation for Fe I lines).

Other ions, as a rule, have lines with smaller equivalent widths (i.e. they should be less affected by departures from LTE). Abundances of these elements were found as direct mean values from all appropriate lines. For Ca and Sc intermediate strength lines are not numerous, while

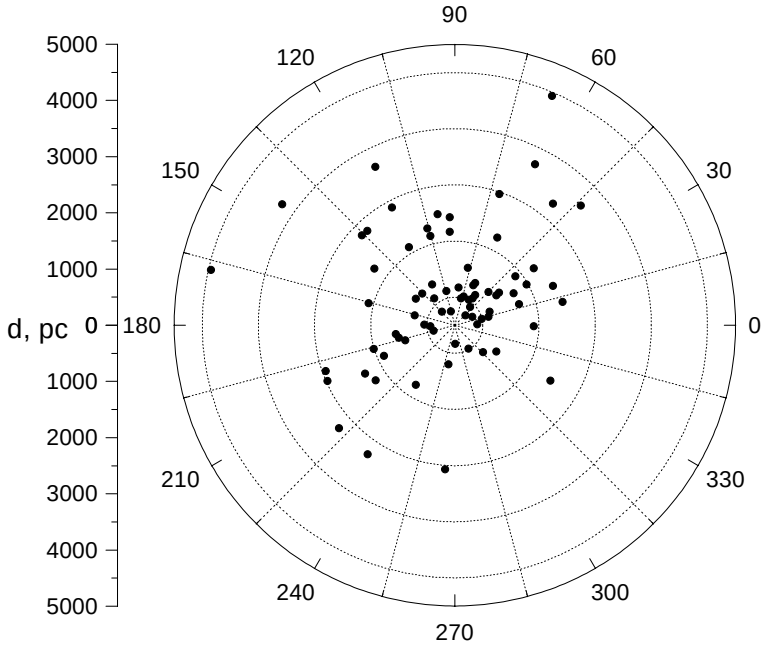

Fig. 4. The distribution of the program Cepheids in the galactic plane.

weak lines are often absent. For these two elements abundance corrections were not determined. Therefore, their abundances should be interpreted with caution.

5. Distances

Galactocentric distances for the program Cepheids were calculated from the following formula (the distances are given in pc):

$$R_{\rm G} = \left[R_{\rm G,\odot}^2 + (d\cos b)^2 - 2R_{\rm G,\odot} d\cos b\cos l\right]^{1/2} \qquad (1)$$

where $R_{\rm G,\odot}$ is the galactocentric distance of the Sun, d is the heliocentric distance of the Cepheid, l is the galactic longitude, and b is the galactic latitude. The heliocentric distance d is given by

$$d = 10^{-0.2(M_{\rm v} - <V> - 5 + A_{\rm v})}. \qquad (2)$$

To estimate the heliocentric distances of program Cepheids we used the "absolute magnitude – pulsational period" relation of Gieren et al. (1998). $E(B-V)$, $<B-V>$, mean visual magnitudes and pulsational periods are from Fernie et al. (1995), see Table 3. We use for $A_{\rm v}$ an expression from Laney & Stobie (1993):

$$A_{\rm v} = [3.07 + 0.28(B-V)_0 + 0.04E(B-V)]\,E(B-V)\cdot(3)$$

For s-Cepheids (DCEPS type) the observed periods are those of the first overtone (see, e.g. Christensen-Dalsgaard & Petersen 1995). Therefore, for these stars the corresponding periods of the unexcited fundamental mode were found using the ratio $P_1/P_0 \approx 0.72$, and these periods were then used to estimate the absolute magnitudes. In the case of V473 Lyr, the fundamental period P_0 was found assuming that this star pulsates in the second overtone (Andrievsky et al. 1998), i.e. $P_1/P_0 = 0.56$. For V924 Cyg and V340 Nor, whose association with the group of s-Cepheids is not certain, we used the observed periods as the fundamental period in order to estimate $M_{\rm v}$.

The galactocentric distance of the Sun $R_{\rm G,\odot} = 7.9$ kpc was adopted from the recent determination by McNamara et al. (2000). Estimated distances and other useful characteristics of our program Cepheids are gathered in Table 3. Because our spectra were obtained with different spectrographs having differing resolving powers, and also because for different stars we have a differing number of spectra (as a rule, one spectrum for Cepheids observed with 6-m telescope), we have assigned for each star a weight in the derivation of the gradient solution. We assigned a weight $W = 1$ to the following stars: those observed with the 6-m telescope (lower resolution spectra), the two stars observed by Harris & Pilachowski (1984), and the stars with one high resolution spectrum, but a low S/N ratio (VX Pup, CV Mon and MY Pup). For the rest of the program stars a weight $W = 3$ was used. The weights are given in the last column of Table 3. The distribution of the analyzed Cepheids in the galactic plane is shown in Fig. 4.

6. Results and discussion

6.1. The radial distribution of elemental abundances: General picture and remarks on some elements

Using our calculated galactocentric distances and average abundances we can determine the galactic metallicity gradient from a number of species. Plots for several chemical elements and results of a linear fit are given in Fig. 5 (iron) and Figs. 6–9 (other elements). Note that, in the plots for Si and Cr, TX Del is not included. This star shows rather strong excess in the abundances of these elements

Table 3. Some physical and positional characteristics of program Cepheids.

Star	P, d	$< B-V >$	$E(B-V)$	$M_{\rm v}$	d, pc	l	b	$R_{\rm G}$, kpc	<[Fe/H]>	W
V473 Lyr (s)	2.6600	0.632	0.026	−2.47	517.2	60.56	7.44	7.66	−0.06	3
SU Cas (s)	2.7070	0.703	0.287	−2.49	322.7	133.47	8.52	8.12	−0.01	3
EU Tau (s)	2.9200	0.664	0.172	−2.58	1058.2	188.80	−5.32	8.94	−0.06	3
IR Cep (s)	2.9360	0.870	0.411	−2.59	624.4	103.40	4.91	8.07	−0.01	1
TU Cas	2.1393	0.582	0.115	−2.21	821.4	118.93	−11.40	8.32	+0.03	3
DT Cyg (s)	3.4720	0.538	0.039	−2.79	487.4	76.55	−10.78	7.80	+0.11	3
V526 Mon (s)	3.7150	0.593	0.093	−2.87	1716.6	215.13	1.81	9.36	−0.13	1
V351 Cep (s)	3.8970	0.940	0.400	−2.93	1640.5	105.20	−0.72	8.48	+0.03	1
VX Pup	3.0109	0.610	0.136	−2.62	1265.5	237.02	−1.30	8.65	−0.13	1
SZ Tau (s)	4.3730	0.844	0.294	−3.07	536.5	179.48	−18.74	8.41	+0.08	3
V1334 Cyg(s)	4.6290	0.504	0.000	−3.14	633.2	83.60	−7.95	7.85	−0.04	3
BG Cru (s)	4.6430	0.606	0.053	−3.14	491.2	300.42	3.35	7.66	−0.02	3
BD Cas (s)	3.6510	–	0.734	−3.25	2371.5	118.00	−0.96	9.25	−0.07	1
RT Aur	3.7282	0.595	0.051	−2.88	428.2	183.15	8.92	8.32	+0.06	3
DF Cas	3.8328	1.181	0.599	−2.91	2297.9	136.00	1.53	9.68	+0.13	1
SU Cyg	3.8455	0.575	0.096	−2.91	781.5	64.76	2.50	7.60	−0.00	3
ST Tau	4.0343	0.847	0.355	−2.97	1020.7	193.12	−8.05	8.89	−0.05	3
V1726 Cyg(s)	5.8830	0.885	0.312	−3.43	1916.2	92.50	−1.61	8.21	−0.02	1
BQ Ser	4.2709	1.399	0.841	−3.04	911.7	35.13	5.37	7.18	−0.04	3
Y Lac	4.3238	0.731	0.217	−3.05	1996.6	98.72	−4.03	8.43	−0.09	3
T Vul	4.4355	0.635	0.064	−3.09	532.7	72.13	−10.15	7.76	+0.01	3
FF Aql (s)	6.2100	0.756	0.224	−3.49	424.4	49.20	6.36	7.63	+0.02	3
CF Cas	4.8752	1.174	0.566	−3.20	3145.2	116.58	−0.99	9.72	−0.01	3
TV Cam	5.2950	1.198	0.644	−3.30	3739.1	145.02	6.15	11.15	−0.06	1
BG Lac	5.3319	0.949	0.336	−3.31	1656.6	92.97	−9.26	8.15	−0.01	3
Del Cep	5.3663	0.657	0.092	−3.31	247.9	105.19	0.53	7.97	+0.06	3
V1162 Aql(s)	7.4670	0.900	0.205	−3.71	1470.2	29.40	−18.60	6.72	+0.01	3
CV Mon	5.3789	1.297	0.714	−3.32	1809.1	208.57	−1.79	9.53	−0.03	1
V Cen	5.4939	0.875	0.289	−3.34	702.3	316.40	3.31	7.41	+0.04	3
V924 Cyg	5.5710	0.847	0.258	−3.36	4428.4	66.90	5.33	7.38	−0.09	1
MY Pup (s)	7.9100	0.631	0.064	−3.78	708.4	261.31	−12.86	8.03	−0.12	1
Y Sgr	5.7734	0.856	0.205	−3.40	496.1	12.79	−2.13	7.42	+0.06	3
EW Sct	5.8233	1.725	1.128	−3.41	345.0	25.34	−0.09	7.59	+0.04	3
FM Aql	6.1142	1.277	0.646	−3.47	842.3	44.34	0.89	7.32	+0.08	3
TX Del	6.1660	0.766	0.132	−3.48	2782.5	50.96	−24.26	6.60	+0.24	3
V367 Sct	6.2931	1.769	1.130	−3.51	1887.7	21.63	−0.83	6.18	−0.01	3
X Vul	6.3195	1.389	0.848	−3.51	831.6	63.86	−1.28	7.57	+0.08	3
AW Per	6.4636	1.055	0.534	−3.54	724.9	166.62	−5.39	8.60	+0.01	3
U Sgr	6.7452	1.087	0.403	−3.59	620.5	13.71	−4.46	7.30	+0.04	3
V496 Aql (s)	9.4540	1.146	0.413	−4.00	1195.1	28.20	−7.13	6.88	+0.05	3
Eta Aql	7.1767	0.789	0.149	−3.66	260.1	40.94	−13.07	7.71	+0.05	3
BB Her	7.5080	1.100	0.414	−3.72	3091.7	43.30	6.81	6.04	+0.15	3
RS Ori	7.5669	0.945	0.389	−3.73	1498.9	196.58	0.35	9.35	−0.10	3
V440 Per (s)	10.5140	0.873	0.273	−4.12	801.1	135.87	−5.17	8.49	−0.05	3
W Sgr	7.5949	0.746	0.111	−3.73	405.4	1.58	−3.98	7.50	−0.01	3
RX Cam	7.9120	1.193	0.569	−3.78	833.4	145.90	4.70	8.60	+0.03	3
W Gem	7.9138	0.889	0.283	−3.78	916.9	197.43	3.38	8.78	−0.04	3
U Vul	7.9906	1.275	0.654	−3.79	570.9	56.07	−0.29	7.60	+0.05	3
DL Cas	8.0007	1.154	0.533	−3.79	1602.1	120.27	−2.55	8.82	−0.01	3
AC Mon	8.0143	1.165	0.508	−3.80	2754.8	221.80	−1.86	10.12	−0.07	1
V636 Cas (s)	11.6350	1.391	0.786	−4.25	592.2	127.50	1.09	8.27	+0.06	3
S Sge	8.3821	0.805	0.127	−3.85	648.1	55.17	−6.12	7.55	+0.10	3
GQ Ori	8.6161	0.976	0.279	−3.88	2437.6	199.77	−4.42	10.22	−0.03	1
V500 Sco	9.3168	1.276	0.599	−3.98	1406.1	359.02	−1.35	6.49	−0.02	3
FN Aql	9.4816	1.214	0.510	−4.00	1383.2	38.54	−3.11	6.87	−0.02	3
YZ Sgr	9.5536	1.032	0.292	−4.01	1205.4	17.75	−7.12	6.77	+0.05	3
S Nor	9.7542	0.941	0.215	−4.03	879.6	327.80	−5.39	7.17	+0.05	3
Beta Dor	9.8424	0.807	0.044	−4.04	335.8	271.73	−32.78	7.90	−0.01	3
Zeta Gem	10.1507	0.798	0.018	−4.08	387.2	195.75	11.90	8.27	+0.04	3
Z Lac	10.8856	1.095	0.404	−4.17	1782.4	105.76	−1.62	8.56	+0.01	3
VX Per	10.8890	1.158	0.515	−4.17	2283.5	132.80	−2.96	9.60	−0.05	3
V340 Nor(s:)	11.2870	1.149	0.332	−4.21	1976.1	329.80	−2.23	6.27	+0.00	3
RX Aur	11.6235	1.009	0.276	−4.24	1579.0	165.77	−1.28	9.44	−0.07	3
TT Aql	13.7547	1.292	0.495	−4.45	976.1	36.00	−3.14	7.13	+0.11	3
SV Mon	15.2328	1.048	0.249	−4.57	2472.3	203.74	−3.67	10.21	−0.03	3
X Cyg	16.3863	1.130	0.288	−4.66	1043.5	76.87	−4.26	7.73	+0.12	3
RW Cam	16.4148	1.351	0.649	−4.66	1748.4	144.85	3.80	9.38	+0.04	3
CD Cyg	17.0740	1.266	0.514	−4.71	2462.1	71.07	1.43	7.47	+0.07	3
Y Oph (s)	23.7880	1.377	0.655	−5.11	664.9	20.60	10.12	7.29	+0.05	3
SZ Aql	17.1408	1.389	0.641	−4.71	1731.0	35.60	−2.34	6.57	+0.15	3
YZ Aur	18.1932	1.375	0.565	−4.78	4444.7	167.28	0.94	12.27	−0.05	1
WZ Sgr	21.8498	1.392	0.467	−5.00	1967.5	12.11	−1.32	5.99	+0.17	3
SW Vel	23.4410	1.162	0.349	−5.09	2572.4	266.20	−3.00	8.47	+0.01	3
X Pup	25.9610	1.127	0.443	−5.21	2776.6	236.14	−0.78	9.72	−0.03	3
T Mon	27.0246	1.166	0.209	−5.26	1369.7	203.63	−2.55	9.17	+0.13	3
SV Vul	44.9948	1.442	0.570	−5.87	1729.5	63.95	0.32	7.31	+0.03	3
S Vul	68.4640	1.892	0.827	−6.38	3199.7	63.45	0.83	7.07	−0.02	3

which could be connected with its peculiar nature (in Harris & Welch 1989 TX Del is reported as a spectroscopic binary. It has also been labeled a Type II Cepheid at times). In the plot for carbon we did not include the data for FN Aql and SV Mon, both of which have an extremely low carbon abundances. These two unusual Cepheids will be discussed in detail in a separate paper.

The information in the plots and also in Fig. 10 enables one to put together several important conclusions. Most radial distributions of the elements studied indicate a negative gradient ranging from about -0.02 dex kpc^{-1} to -0.06 dex kpc^{-1}, with an average of -0.03 dex kpc^{-1} for the elements in Figs. 5–8. The most reliable value comes from iron (typically the number of iron lines for each star is about 200–300). The gradient in iron is -0.029 dex kpc^{-1},

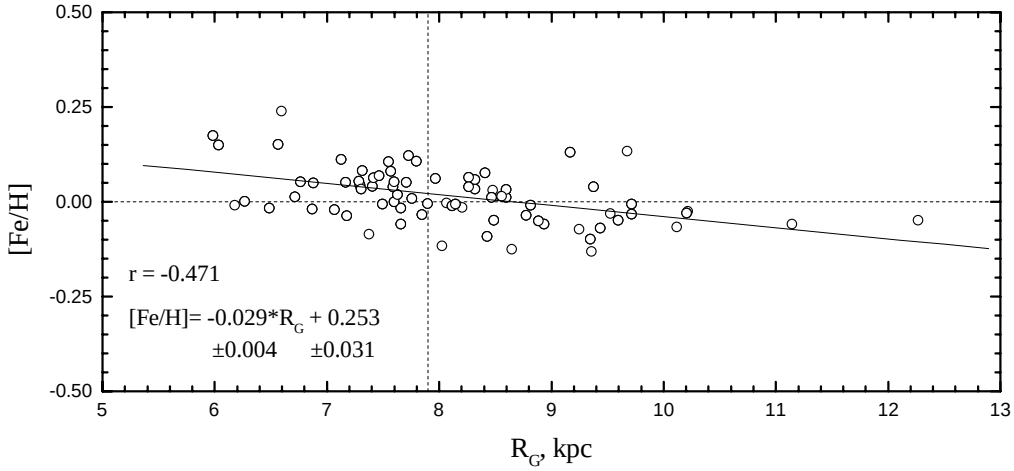

Fig. 5. Iron abundance gradient and its linear approximation. The position of the Sun is at the intersection of the dashed lines.

which is close to the typical gradient value produced by other iron-group elements. Examination of Fig. 5 might lead one to suspect that the iron gradient is being controlled by the cluster of stars at $R \approx 6.5$ with [Fe/H] ≈ 0.2. If one deletes these stars from the solution the gradient falls to approximately -0.02 dex kpc^{-1}. This latter value differs from the value determined using all the data by about twice the formal uncertainty in either slope. However, we do not favour the neglect these points as there is no reason to suspect these abundances relative to the bulk of the objects. Indeed, in a subsequent paper, we shall present results for Cepheids which lie closer to the galactic center and which have abundances above those of this study, which may imply a steepening of the gradient towards the galactic center.

Unweighted iron abundances give a gradient of -0.028 dex kpc^{-1}. Both weighted and unweighted iron gradients are not significantly changed if we remove two Cepheids at galactocentric distances greater than 11 kpc (gradient is -0.031 dex kpc^{-1}). Thus, the average slope of about -0.03 dex kpc^{-1} probably applies to the range $6 \leq R_{\rm G}$ (kpc) ≤ 10. Notice that in all cases the correlation coefficient is relatively low, $r \approx 0.47$.

Carbon shows a surprisingly clear dependence upon galactocentric distance (Fig. 6a): the slope of the relation is among the largest from examined elements. We have included in the present study elements such as carbon and sodium, although the gradients based on their abundances determined from Cepheids may not be conclusive. In fact, it is quite likely that the surface abundances of these elements have been altered in these intermediate mass stars during their evolution from the main sequence to the Cepheid stage. For example, the surface abundance of carbon should be decreased after the global mixing which brings the CNO-processed material into the stellar atmosphere (turbulent diffusion in the progenitor B main sequence star, or the first dredge-up in the red giant phase). Some decrease in the surface abundance of oxygen is also expected for supergiant stars, but at a significantly lower level than for carbon (Schaller et al. 1992).

It is also well known that galactic supergiants (Cepheids, in particular) show an increased sodium abundance which is usually interpreted as a result of dredge-up of material processed in the Ne–Na cycle (and therefore enriched in sodium) to the stellar surface (Sasselov 1986; Luck 1994; Denissenkov 1993a, 1993b, 1994). Such a contamination of the Cepheids' atmospheres with additional sodium may result in a bias of the [Na/H] gradient value derived from Cepheids in relation to the true gradient. It can be seen that our results in Figs. 6a,c are consistent with these considerations on C and Na, respectively. It is not clear how these effects should affect stars at different galactocentric distances (with different metallicities), but it is likely that they contribute to increase the dispersion in the abundances, thus producing a flatter gradient.

There are some indications (Andrievsky & Kovtyukh 1996) that surface Mg and Al abundances in yellow supergiants can be altered to some extent due to mixing of the material processed in the Mg–Al cycle with atmospheric gas. This supposition seems to gain some additional support from our present data (see Fig. 11) where one can see that the Mg and Al abundances are correlated.

As surface abundance modifications depend upon the number of visits to the red giant region (i.e. the number of dredge-up events) as well as other factors (pre dredge-up events, depth of mixing events, mass), it is possible that the program Cepheids could show differential evolutionary effects in their abundances. Because of the high probability of such effects impacting the observed carbon and sodium (and perhaps, oxygen, magnesium, and aluminum) abundances in these Cepheids, we recommend that our gradient values for carbon and sodium to be viewed with extreme caution, while the gradients of oxygen, magnesium and aluminum abundances could be used, but also with some caution.

The difference in metallicity between the stars of our sample (say, at 6 kpc and 10 kpc) is about 0.25 dex. This is a rather small value to detect/investigate the so-called "odd-even" effect, that is the metallicity dependent yield for some elements which should be imprinted on

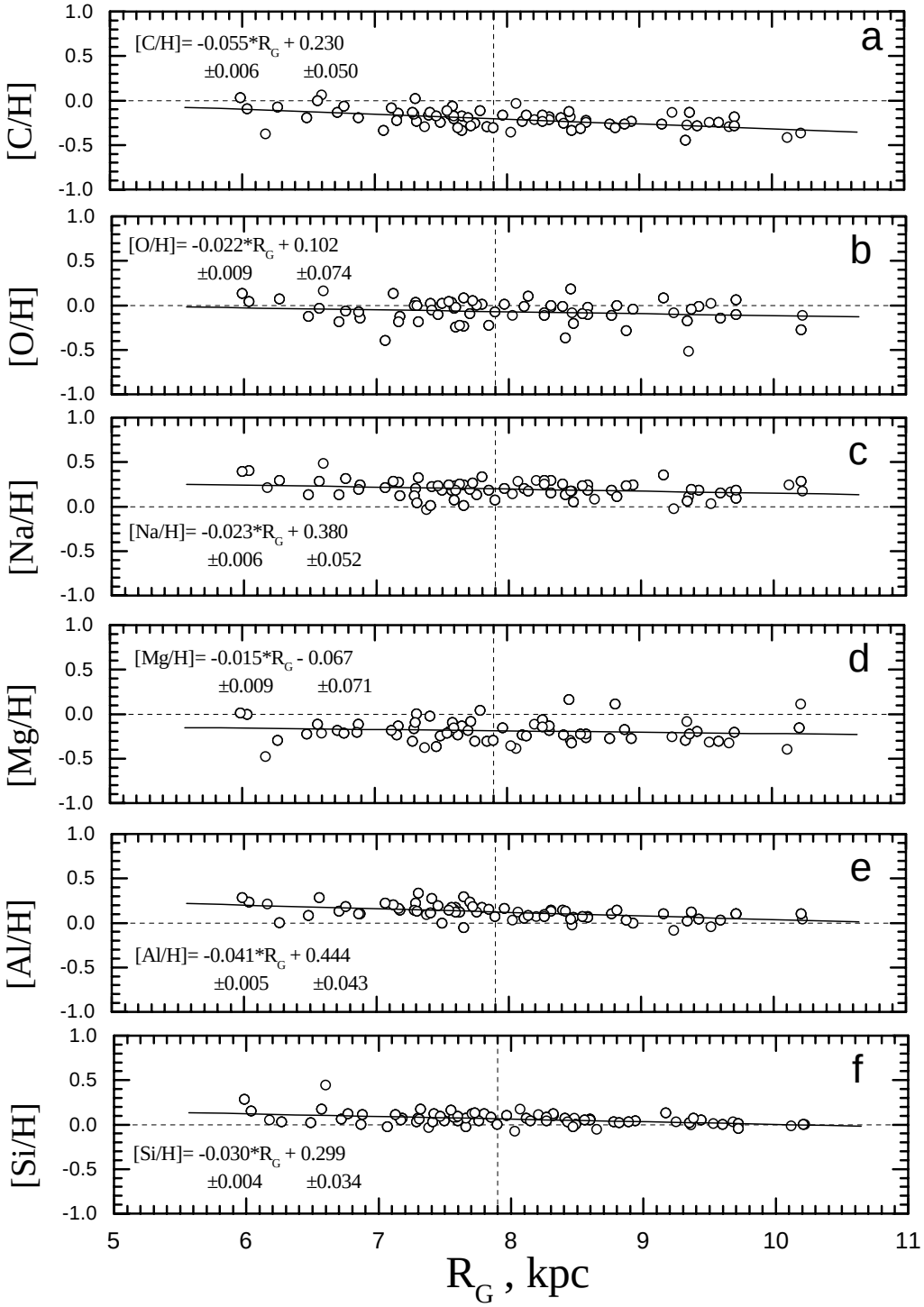

Fig. 6. Abundance gradients for other investigated elements: C–Si.

the trends of abundance ratios for [El_{odd}/El_{even}] versus galactocentric distance, see for details Hou et al. (2000). Such elements as, for example, aluminum, scandium, vanadium and manganese should show progressively decreasing abundances with overall metal decrease. This should manifest itself as a gradient in [El_{odd}/Fe]. We have plotted the abundance ratios for some "odd" elements (normalized to iron abundance) versus R_G in Fig. 12. As one can see, none of the abundance ratios plotted versus galactocentric distance shows a clear dependence upon R_G. This could mean that the "odd-even" effect may be overestimated if only the yields from massive stars are taken into account ignoring other possible sources, or that the effect is not sufficiently large to be seen over the current distance and metallicity baseline.

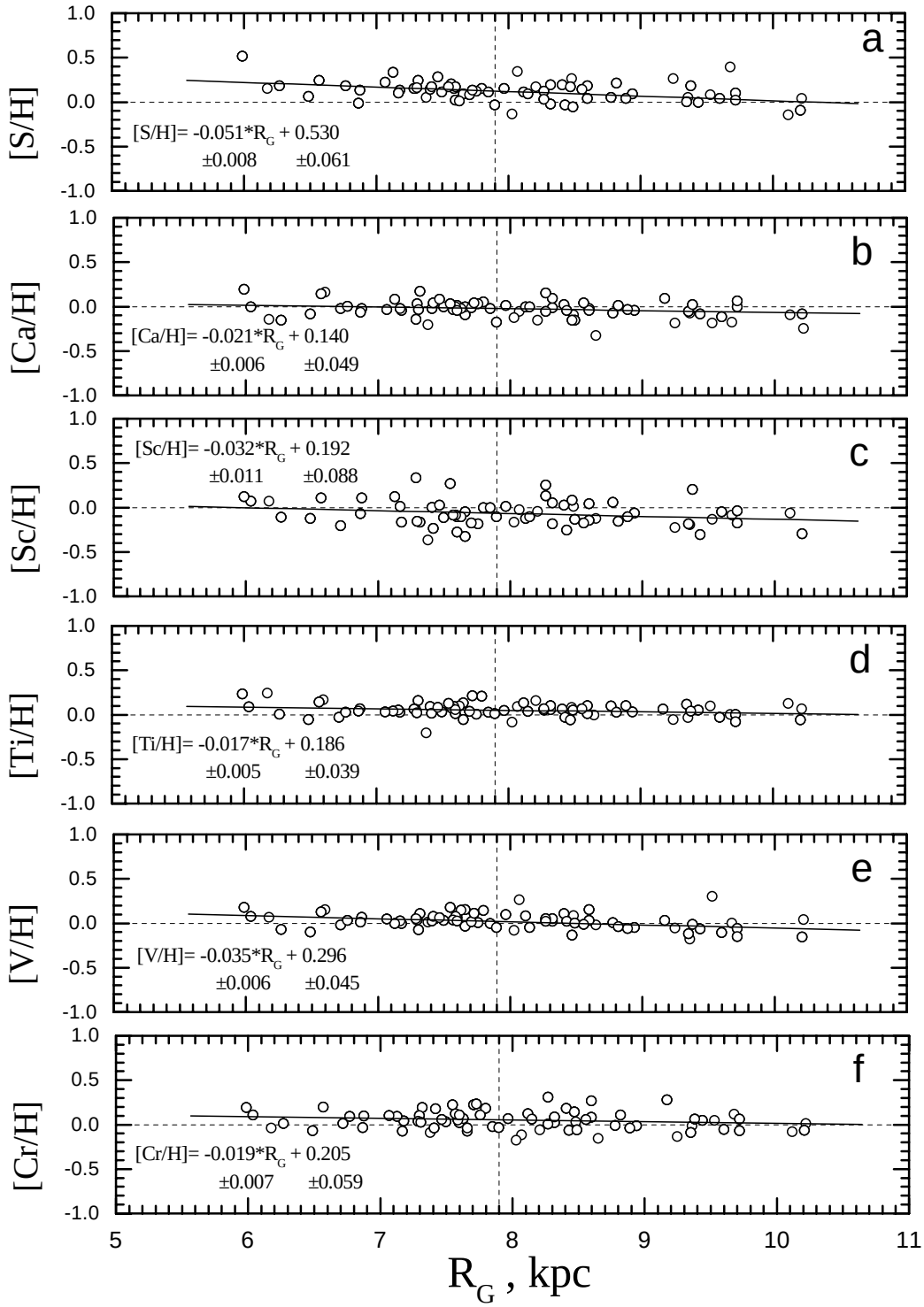

Fig. 7. Same as Fig. 6, but for S–Cr.

6.2. Metallicity dispersion and the metallicity in the solar vicinity

There is a spread in the metallicity at each given galactocentric distance (larger than the standard error of the abundance analysis) which is most likely connected with local inhomogeneities in the galactic disc. As an example, in Fig. 13, we show the derived iron abundance vs. galactic longitude for the stars of our sample (a few Cepheids with heliocentric distances large than 3000 pc were excluded). The distribution gives only a small hint about a local increase of the metallicity in the solar vicinity towards the direction $l \approx 30°$ and $150°$.

It is important to note that at the solar galactocentric distance those elements, whose abundance is not supposed

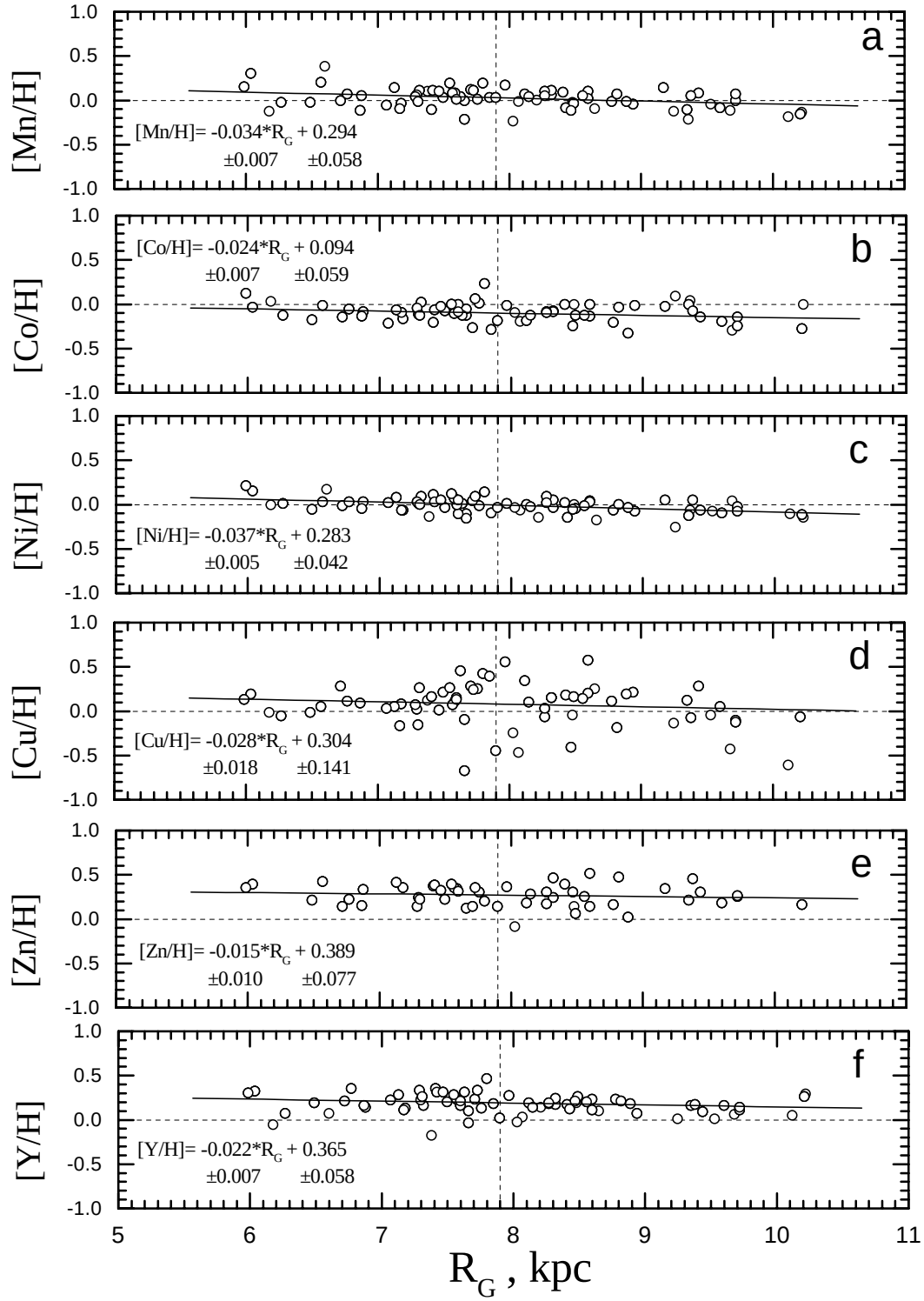

Fig. 8. Same as Fig. 6, but for Mn–Y.

to be changed in supergiants during their evolution, show on average the solar abundance in Cepheids. Relative to the solar region, the stars within our sample which are within 500 pc of the Sun have a mean [Fe/H] of $\approx +0.01$ ($n = 14$, $\sigma = 0.06$). If we consider all program stars at a galactocentric radius of 7.4–8.4 kpc, i.e. those in a 1 kpc wide annulus centered at the solar radius, we find a mean [Fe/H] of approximately +0.03 ($n = 29$, $\sigma = 0.05$).

This result again stresses the importance of the problem connected with subsolar metallicities reported for the hot stars from the solar vicinity (see, e.g. Gies & Lambert 1992; Cunha & Lambert 1994; Kilian 1992; Kilian et al. 1994; Daflon et al. 1999; Andrievsky et al. 1999). This also follows from the plots provided by Gummersbach et al. (1998) for several elements.

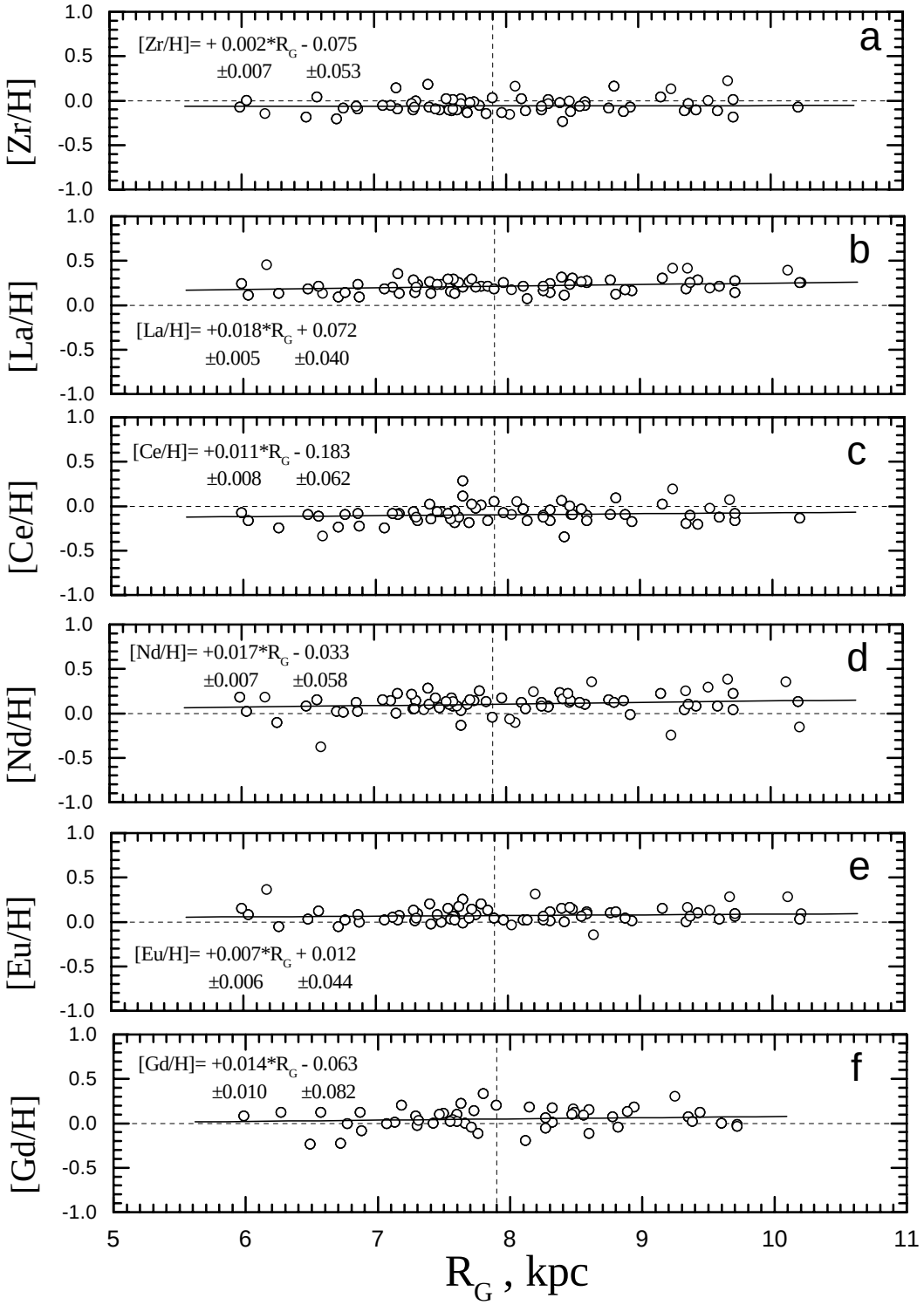

Fig. 9. Same as Fig. 6, but for Zr–Gd.

This problem was discussed, for instance, by Luck et al. (2000). The authors compared the elemental abundances of B stars from the open cluster M 25 with those of the Cepheid U Sgr and two cool supergiants which are also members of the cluster, and found disagreement in the abundances of the B stars and supergiants; e.g., while the supergiants of M 25 show nearly solar abundances, the sample of B stars demonstrate a variety of patterns from under- to over-abundances. This should not be observed if we assume that all stars in the cluster were born from the same parental nebula. Obviously, the problem of some disagreement between abundance results from young supergiants and main-sequence stars requires further investigation.

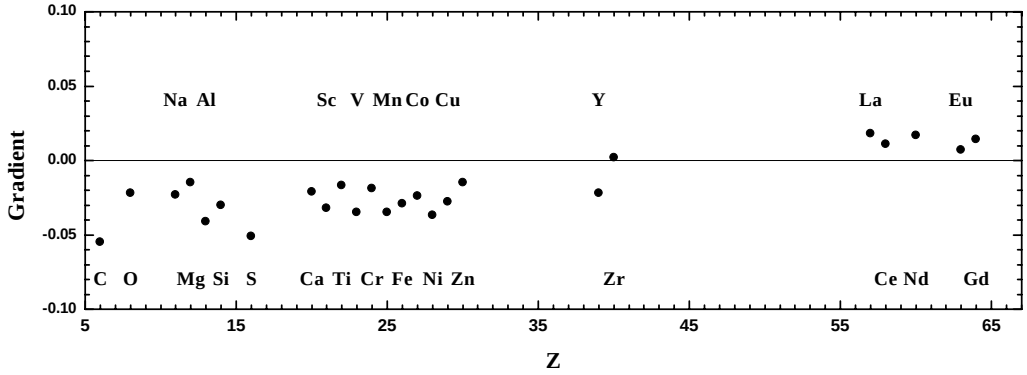

Fig. 10. Derived gradients versus atomic number.

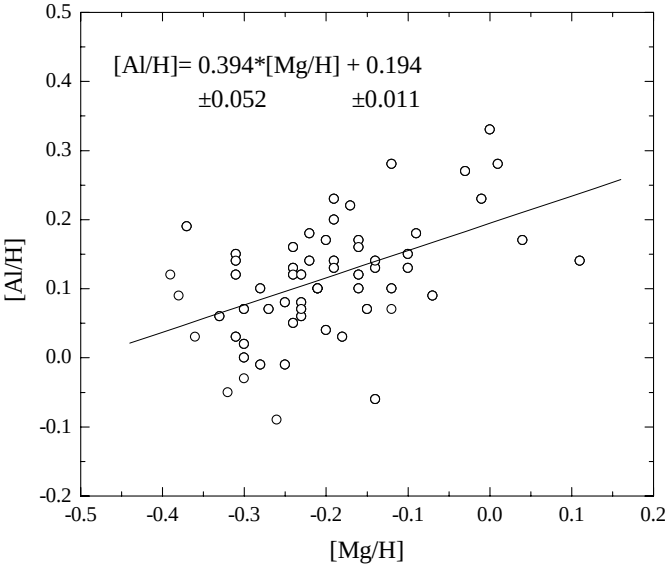

Fig. 11. [Al/H] vs. [Mg/H] for program Cepheids.

6.3. Flattening of the elemental distribution in the solar neighbourhood

All previous studies of the radial abundance distribution in the galactic disc have considered only chemical elements from carbon to iron, and all derived gradients have shown a progressive decrease in abundance with increasing galactocentric distance. For the elements from carbon to yttrium in this study our gradient values also have negative signs, while for the heavier species (from zirconium to gadolinium) we obtained (within the error bars) near-to-zero gradients (see Fig. 10). Two obvious features which are inherent to derived C-Gd abundance distributions have to be interpreted: a rather flat character of the distribution for light/iron-group elements, and an apparent absence of a clear gradient for heavy species.

The flattening of the abundance distribution can be caused by radial flows in the disc which may lead to a homogenization of ISM. Among the possible sources forcing gas of ISM to flow in the radial direction, and therefore producing a net mixing effect there could be a gas viscosity in the disc, gas infall from the halo, gravitational interaction between gas and spiral waves or a central bar (see e.g., Lacey & Fall 1985; Portinari & Chiosi 2000).

The mechanism of the angular momentum redistribution in the disc based on the gas infall from the halo is dependent upon the infall rate, and therefore it should have been important at the earlier stages of the Galaxy evolution, while other sources of the radial flows should effectively operate at present.

Gravitational interaction between the gas and density waves produces the radial flows with velocity (Lacey & Fall 1985):

$$v_{\rm r} \sim (\Omega_{\rm p} - \Omega_{\rm c})^{-1}, \qquad (4)$$

where $\Omega_{\rm p}$ and $\Omega_{\rm c}$ are the angular velocities of the spiral wave and the disc rotation respectively. According to Amaral & Lépine (1997) and Mishurov et al. (1997) among others, based on several different arguments, the galactic co-rotation resonance is located close to the solar galactic orbit. The co-rotation radius is the radius at which the galactic rotation velocity coincides with the rotation velocity of the spiral pattern. Together with Eq. (4) this means that, inside the co-rotation circle, gas flows towards the galactic center ($\Omega_{\rm c} > \Omega_{\rm p}$ and $v_{\rm r} < 0$), while outside it flows outwards. This mechanism can produce some "cleaning" effect in the solar vicinity, and thus can lead to some flattening of the abundance distribution. In addition, it could explain the similarity in the solar abundances and mean abundances in the five billion years younger Cepheids located at the solar galactocentric annulus (see Fig. 5), although one might expect that the Cepheids from this region should be more abundant in metals than our Sun.

There is a clear evidence that the bars of spiral galaxies have also a great impact on chemical homogenization in the discs (Edmunds & Roy 1993; Martin & Roy 1994; Gadotti & Dos Anjos 2001). It has been shown that a flatter abundance gradient is inherent to galaxies which have a bar structure. This could imply that a rotating bar is capable of producing significant homogenization of the interstellar medium, while such homogenization is not efficient in unbarred spiral galaxies.

The direct detection of a bar at the center of our galaxy using *COBE* maps was reported by

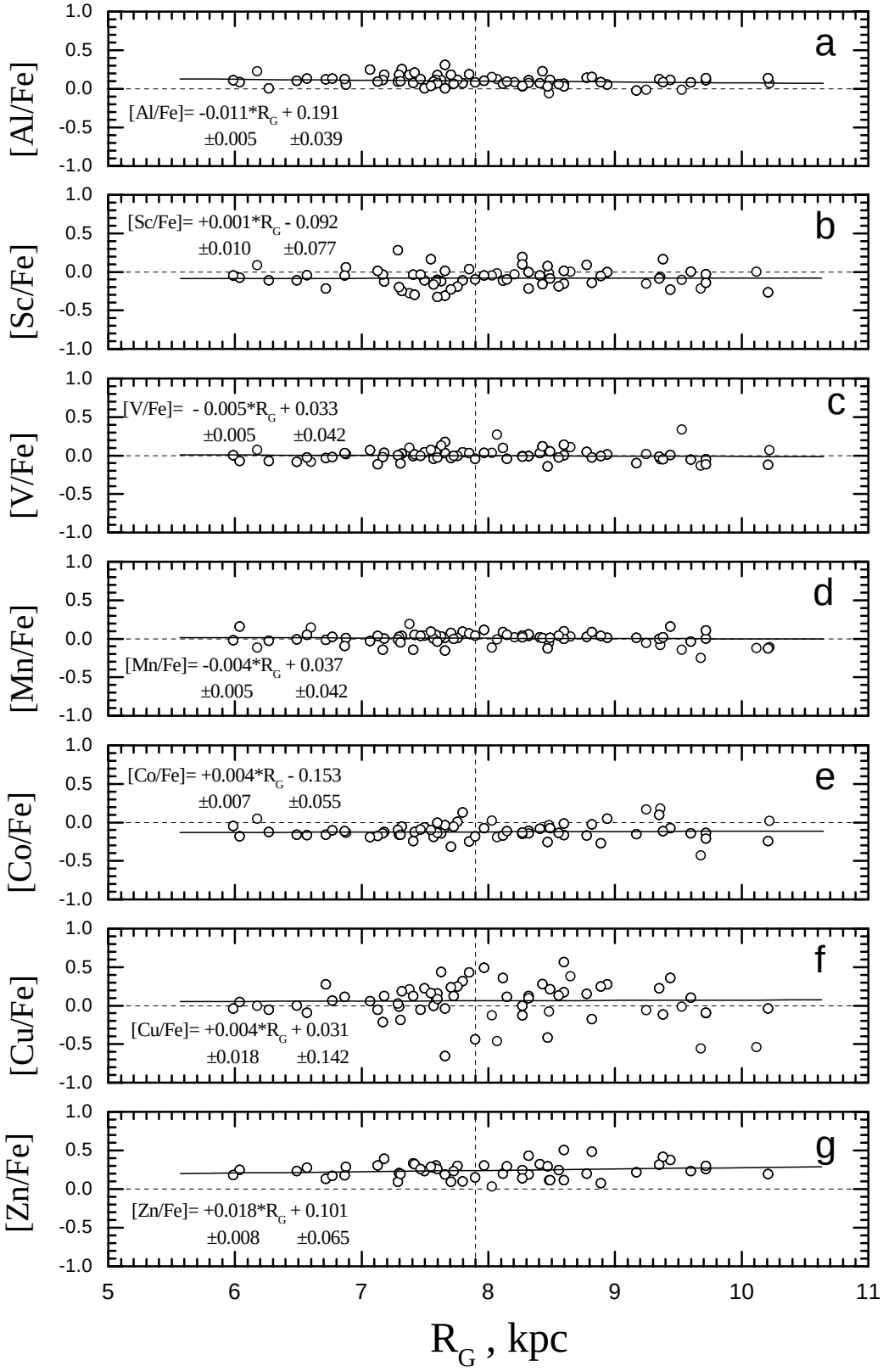

Fig. 12. Gradients for some abundance ratios.

Blitz & Spergel (1991). Kuijken (1996), Gerhard (1996), Gerhard et al. (1998), Raboud et al. (1998) also suggest that the Milky Way is a barred galaxy. The most recent evidence for a long thin galactic bar was reported by López-Corredoira et al. (2001) from the DENIS survey. These authors conclude that our Galaxy is a typical barred spiral. If so, then the Milky Way should obey the relation between the slope of metallicity distribution and the bar

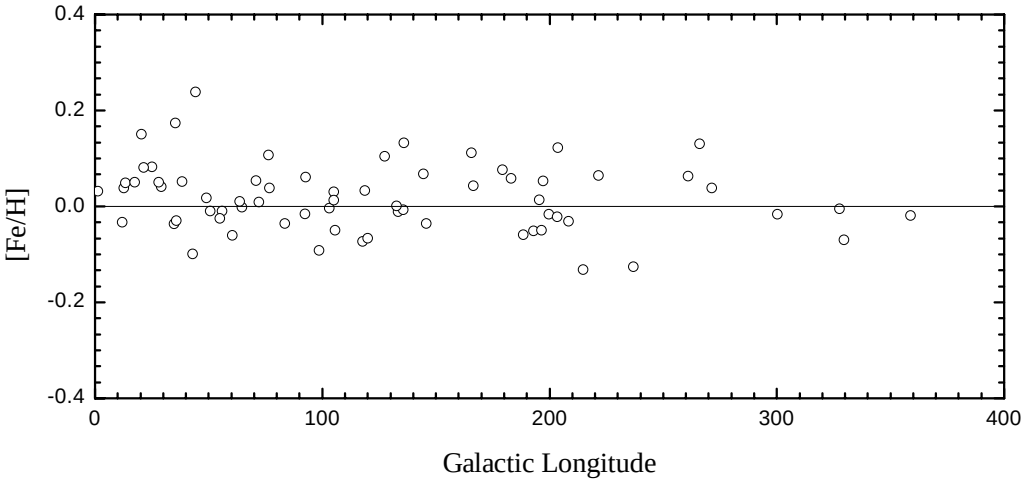

Fig. 13. Iron abundance vs. galactic longitude.

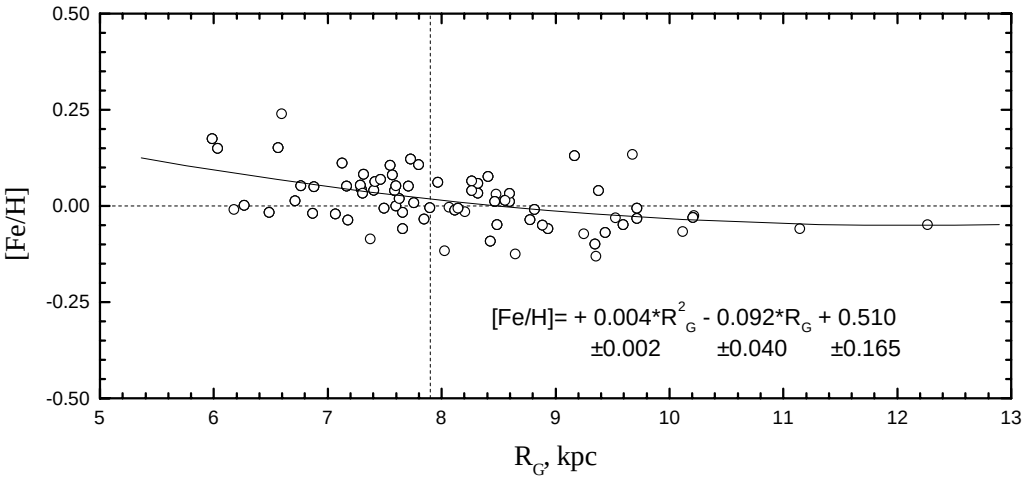

Fig. 14. Iron abundance profile with a parabolic approximation.

strength (specifically, the axial ratio), which is based on the data obtained from other galaxies.

According to the above mentioned authors the galactic bar is triaxial and has an axial ratio (b/a) of about 1/3−1/2 (see also Fux 1997, 1999). With such axial ratio an ellipticity $E_B = 10(1-b/a) \approx 5-7$. Lépine & Leroy (2000) presented a model which reproduces a near-infrared brightness distribution in the Galaxy. Their estimate of the galactic bar characteristics supposes that the total length of the bar should be about 4.6 kpc, while its width about 0.5 kpc. In this case an ellipticity could be even larger than 7. For such ellipticities the observational calibration of Martin & Roy (1994) for barred galaxies predicts a metallicity slope of about −0.03 to ≈0 dex kpc^{-1} for oxygen. Our results on abundance gradients in the solar neighbourhood for iron-group elements and light species (such as Si, Ca, and even oxygen) appear to be in good agreement with expected gradient value which is estimated for the galactic disc solely from bar characteristics.

Martinet & Friedli (1997) investigated secular chemical evolution in barred systems and found that a strong bar is capable of producing significant flattening of the initial gradient across the disc. Using numerical results of that paper one can trace the (O/H) abundance evolution in barred systems. With our abundance gradients for such elements as oxygen, silicon, calcium and iron-group elements one can conclude that an expected age of the galactic bar is approximately 1 Gyr, or less. Another important result obtained by Martinet & Friedli (1997) is that the bar of such an age should produce not only significant flattening across almost the whole disc, but also steepening of the abundance distribution in the inner parts (our observational results for this region will be discussed in the next paper from this series).

An additional mechanism which may cause some local flattening (or even a shallow local minimum in the elemental abundances) should operate near the galactocentric solar radius where the relative rotational velocity of the disc and spiral pattern is small. The shocks that arise when the gas orbiting in the disc penetrates the spiral potential perturbation, and which are responsible for triggering star formation in spiral arms, pass through a minimum strength at this galactic radius, due to almost

zero relative velocity. Furthermore, simulations performed by Lépine et al. (2001) show that there is also a gas depletion at the co-rotation radius. Both reasons point towards a minimum of star formation rate at the co-rotation radius. This lower star formation rate manifests itself in the models as a minimum in elemental abundances. One can expect that after a few billion years, a galactic radius with minimum star formation rate should correspond to a local minimum in metallicity. The flat local minimum in metal abundance should be observable, unless the mechanisms that produce radial transport or radial mixing of the gas in the disc are important, or if the co-rotation radius varied appreciably in a few billion years. Note that the star-formation rate also depends on the gas density, which decreases towards large galactic radii. The combined effect of gas density and co-rotation could produce a slightly displaced minimum.

At first glance, the abundance data presented in Figs. 5–9 show little indication of a local abundance minimum (or discontinuity) at the solar galactocentric radius. Nevertheless, the parabolic fit of the iron abundance distribution rather well represents observed data, and shows that a small increase in the metallicity at galactic radii larger than the co-rotation radius may not be excluded (Fig. 14).

Comparing gradients from iron-group elements (small and negative) with those from the heaviest species (near to zero) one could propose the following preliminary explanation of the observed difference. The known contributors of the O-to-Fe-peak nuclei to ISM are massive stars exploding as SNe II (short-lived) and SNe I (long-lived), while s-process elements (past iron-peak) are created only in the low-mass AGB stars (1–4 $M_{\odot}$, Travaglio et al. 1999). The extremely flat distribution in the disc seen for s-process elements implies that there should exist some mechanism(s) effectively mixing ISM at time-scales less than the life times of the stars with masses 1–4 $M_{\odot}$ ($\tau \approx 0.3-10$ Gyr). At the same time such a mechanism may not be able to completely erase the O-Fe gradients related to the ISM, and imprinted on the young stars. If the characteristic time of the mixing (even being possibly comparable to the SNe I life time) exceeds a nuclear evolution of the SNe II O-Fe contributors, then these are the high-mass stars that could be responsible for the resulting small negative gradients from O-Fe elements in the disc.

If one adopts the velocity of the radial flows, say, 4 km s^{-1} (see discussion in Lacey & Fall 1985; Stark & Brand 1989), then the necessary time to mix the gas within about 4 kpc (baseline covered by our data) should be likely less than 1 Gyr, that is below the life-time intervals for AGB progenitors with 1–2 $M_{\odot}$. However, this ad hoc supposition meets a problem with the observed Eu gradient. This element is believed to be produced mainly through the r-process in lower-mass SNe II (e.g., Travaglio et al. 1999), and therefore should probably behave similar to, for example, iron, but its radial abundance distribution appears to be quite similar to that of the *s*-process elements, like Zr, La, Ce, Nd (see Fig. 10).

Acknowledgements. SMA would like to express his gratitude to FAPESP for the visiting professor fellowship (No. 2000/06587-3) and to Instituto Astronômico e Geofísico, Universidade de São Paulo for providing facility support during a productive stay in Brazil.

The authors thank Drs. A. Fry and B. W. Carney for the CCD spectra of some Cepheids, Drs. H. C. Harris and C. A. Pilachowski for providing the plate material on two distant Cepheids TV Cam and YZ Aur, Dr. G. A. Galazutdinov for the spectra of V351 Cep, BD Cas and TX Del, Dr. I. A. Usenko, Mrs. L. Yu. Kostynchuk and Mr. Yu. V. Beletsky for the help with data reduction. The authors are also thankful to Dr. Yu. N. Mishurov for discussion and Drs. N. Prantzos, J. L. Hou and C. Bertout for several comments.

We are indebted to the referee, Dr. B. W. Carney, for a detailed reading of the paper, and for his many valuable suggestions and comments which improved the first version.

References

Afflerbach, A., Churchwell, E., & Werner, M. W. 1997, ApJ, 478, 190
Amaral, L. H., & Lépine, J. R. D. 1997, MNRAS, 286, 885
Andrievsky, S. M., & Kovtyukh, V. V. 1996, Ap&SS, 245, 61
Andrievsky, S. M., Kovtyukh, V. V., Bersier, D., et al. 1998, A&A, 329, 599
Andrievsky, S. M., Korotin, S. A., Luck, R. E., & Kostynchuk, L. Yu. 1999, A&A, 342, 756
Andrievsky, S. M., Kovtyukh, V. V., Korotin, S. A., Spite, M., & Spite, F. 2001, A&A, 367, 605
Barklem, P. S., Piskunov, N., & O'Mara, B. J. 2000, A&A, 142, 467
Blitz, L., & Spergel, D. N. 1991, ApJ, 379, 631
Cameron, L. M. 1985, A&A, 147, 47
Carraro, G., Ng, Yu. K., & Portinari, L. 1998, MNRAS, 296, 1045
Castelli, F. 1996, Model atmospheres and stellar spectra, ed. S. J. Adelman, F. Kupka, & W. W. Weiss (San Francisco), ASP Conf. Ser., 108, 85
Christensen-Dalsgaard, & Petersen, J. O. 1995, A&A, 299, L17
Cunha, K., & Lambert, D. L. 1994, ApJ, 426, 170
Daflon, S., Cunha, K., & Becker, S. R. 1999, ApJ, 522, 950
Deharveng, L., Peña, M., Caplan, J., & Costero, R. 2000, MNRAS, 311, 329
Dennisenkov, P. A. 1993a, SSR, 66, 405
Dennisenkov, P. A. 1993b, SSR, 74, 363
Dennisenkov, P. A. 1994, A&A, 287, 113
Edmunds, M. G., & Roy, J.-R. 1993, MNRAS, 261, L17
Evans, N. R., & Teays, T. J. 1996, AJ, 112, 761
Fernie, J. D., Evans, N. R., Beattie, B., & Seager, S. 1995, IBVS, 4148, 1
Fernley, J.A., Skillen, I., & Jameson, R. F. 1989, MNRAS, 237, 947
Fich, M., & Silkey, M. 1991, ApJ, 366, 607
Fitzsimmons, A., Brown, P. J. F., Dufton, P. L., & Lennon, D. J. 1990, A&A, 232, 437
Fitzsimmons, A., Dufton, P. L., & Rolleston, W. R. J. 1992, MNRAS, 259, 489
Friel, E. D. 1995, ARA&A, 33, 381
Friel, E. D. 1999, Ap&SS, 265, 271
Friel, E. D., & Janes, K. A. 1993, A&A, 267, 75
Fry, A. M., & Carney, B. W. 1997, AJ, 113, 1073
Fux, R. 1997, A&A, 327, 983

Fux, R. 1999, A&A, 345, 787
Gadotti, D. A., & Dos Anjos, S. 2001, ApJ, in press
Gehren, T., Nissen, P. E., Kudritzki, R. P., & Butler, K. 1985, Proc. ESO Workshop on production and distribution of CNO elements, ed. I. J. Danziger, F. Matteucci, & K. Kjaer (Garching, ESO), 171
Geisler, D., Clariá, J. J., & Minniti, D. 1992, AJ, 104, 1892
Gerhard, O. E. 1996, Unresolved problems of the Milky Way, ed. L. Blitz, & P. Teuben (Kluwer, Dordrecht), 79
Gerhard, O. E., Binney, J. J., & Zhao, H. 1998, Highlights of Astronomy, ed. J. Andersen (Kluwer, Dordrecht), 628
Gieren, W. P., Fouqué, P., & Gómez, M. 1998, ApJ, 496, 17
Gies, D. R., & Lambert, D. L. 1992, ApJ, 387, 673
Gough, D. O., Ostriker, J. P., & Stobie, R. S. 1965, ApJ, 142, 1649
Grevesse, N., Noels, A., & Sauval, J. 1996, ASP Conf. Ser., 99, 117
Gummersbach, C. A., Kaufer, D. R., Schäfer, D. R., Szeifert, T., & Wolf, B. 1998, A&A, 338, 881
Harris, H. C. 1981, AJ, 86, 707
Harris, H. C., & Pilachowski, C. A. 1984, ApJ, 282, 655
Harris, H. C., & Welch, D. L. 1989, AJ, 98, 981
Hill, V., Andrievsky, S. M., & Spite, M. 1995, A&A, 293, 347
Hou, J. L., Prantzos, N., & Boissier, S. 2000, A&A, 362, 921
Janes, K. A. 1979, ApJS, 39, 135
Kaufer, A., Szeifert, T., Krenzin, R., Baschek, B., & Wolf, B. 1994, A&A, 289, 740
Kilian, J. 1992, A&A, 262, 171
Kilian, J., Montenbruck, O., & Nissen, P. E. 1994, A&A, 284, 437
Kilian-Montenbruck, J., Gehren, T., & Nissen, P. E. 1994, A&A, 291, 757
Kiss, L. L. 1998, MNRAS, 297, 825
Kovtyukh, V. V., & Andrievsky, S. M. 1999, A&A, 351, 597
Kovtyukh, V. V., & Gorlova, N. I. 2000, A&A, 358, 587
Kuijken, K. 1996, Barred galaxies, ed. R. Buta, D. A. & Crocker, B. G. Elmegreen (ASP, San Francisco), 504
Kurucz, R. L. 1992, The Stellar Populations of Galaxies, ed. B. Barbuy, & A. Renzini, IAU Symp., 149, 225
Kurucz, R. L., Furenlid, I., Brault, I., & Testerman, L. 1984, The solar flux atlas from 296 nm to 1300 nm, NSO
Lacey, C. G., & Fall, M. 1985, ApJ, 290, 154
Laney, C. D., & Stobie, R. S. 1993, MNRAS, 263, 291
Lépine, J. R. D., & Leroy, P. 2000, MNRAS, 313, 263
Lépine, J. R. D., Mishurov, Yu. N., & Dedikov, S. Yu. 2001, ApJ, 546, 234
López-Corredoira, M., Hammersley, P. L., Garzón, F., et al. 2001, A&A, 373, 139
Luck, R. E. 1982, ApJ, 256, 177
Luck, R. E. 1994, ApJS, 91, 309
Luck, R. E., Andrievsky, S. M., Kovtyukh, V. V., Korotin, S. A., & Beletsky, Yu. V. 2000, A&A, 361, 189
Maciel, W. J., & Köppen, J. 1994, A&A, 282, 436
Maciel, W. J., & Quireza, C. 1999, A&A, 345, 629
Martin, P., & Roy, J.-R. 1994, ApJ, 424, 599
Martinet, L., & Friedli, D. 1997, A&A, 323, 363
McNamara, D. H., Madsen, J. B., Barnes, J., & Ericksen, B. F. 2000, PASP, 112, 202
Mishurov, Yu. N., Zenina, I. A., Dambis, A. K., Mel'nik, A. M., & Rastorguev, A. S. 1997, A&A, 323, 775
Neese, C. L., & Yoss, K. M. 1988, AJ, 95, 463
Panagia, N., & Tosi, M. 1981, A&A, 96, 306
Pasquali, A., & Perinotto, M. 1993, A&A, 280, 581
Peña, M., Deharveng, L., Caplan, J., & Costero, R. 2000, Rev. Mex. Astron. Astrofis., 9, 184
Phelps, R. 2000, Chemical evolution of the Milky Way, ed. F. Matteucci, & F. Giovannelli (Kluwer Dordrecht), 239
Portinari, L., & Chiosi, C. 2000, A&A, 355, 929
Raboud, D., Grenon, M., Martinet, L., Fux, R., & Udry, S. 1998, A&A, 335, L61
Rodriguez, M. 1999, A&A, 351, 1075
Rolleston, W. R. J., Smartt, S. J., Dufton, P. L., & Ryans, R. S. I. 2000, A&A 363, 537
Rudolph, A. L., Simpson, J. P., Haas, M. R., Erickson, E. F., & Fich, M. 1997, ApJ 489, 94
Sasselov, D. D. 1986, PASP, 98, 561
Schaller, G., Shaerer, D., Meynet, G., & Maeder, A. 1992, A&AS, 96, 269
Shaver, P. A., McGee, R. X., Newton, L. M., Danks, A. C., & Pottasch, S. R. 1983, MNRAS, 204, 53
Simpson, J. P., & Rubin, R. H. 1990, ApJ, 354, 165
Simpson, J. P., Colgan, S. W. J., Rubin, R. H., Erickson, E. F., & Haas, M. R. 1995, ApJ, 444, 721
Smartt, S. J., & Rolleston, W. R. J. 1997, ApJ, 481, L47
Stark, A. A., & Brand, J. 1989, ApJ, 339, 763
Thogersen, E. N., Friel, E. D., & Fallon, B. V. 1993, PASP, 105, 1253
Travaglio, C., Galli, D., Gallino, R., et al. 1999, ApJ, 521, 691
Turner, D. G. 1996, JRASC, 90, 82
Vilchez, J. M., & Esteban, C. 1996, MNRAS, 280, 720